J. Fluid Mech. (1997), *vol.* 336, *pp.*1 –32

Steady axisymmetric motion of deformable drops falling or rising through a homoviscous fluid in a tube at intermediate Reynolds number

By LLOYD A. BOZZI [1], JAMES Q. FENG [2]†,
TIMOTHY C. SCOTT [2] AND ARNE J. PEARLSTEIN [1]‡

[1] Department of Mechanical and Industrial Engineering, University of Illinois at
Urbana-Champaign, 1206 West Green Street, Urbana, IL 61801, USA

[2] Chemical Technology Division, Oak Ridge National Laboratory, PO Box 2008, Oak Ridge,
TN 37831, USA

(Received 25 October 1995 and in revised form 11 September 1996)

The steady axisymmetric flow in and around a deformable drop moving under the action of gravity along the axis of a vertical tube at intermediate Reynolds number is studied by solving the nonlinear free-boundary problem using a Galerkin finite-element method. For the case where the drop and suspending liquid have the same viscosity, the ratio of the densities is 6/5 or 5/6, and the radius of the tube is equal to twice the radius of a sphere having the drop volume, four significant results are apparent in the computations. First, we compute drops showing much more deformation, and in particular the development of considerably more non-convexity, than those found in previous calculations for non-zero Reynolds number. The degree of non-convexity typically grows with the Reynolds number. Secondly, external recirculation zones can be attached to or disjoint from the drop. We find when there is a single external recirculation zone, that is disjoint (as found by Dandy & Leal), it can attach to the drop as the Reynolds number is increased. As the Reynolds number further increases, this is immediately followed by division of the drop into two adjacent recirculating regions. Thirdly, we sometimes find two recirculation zones in the suspending liquid. Finally, the drag coefficient, axis ratio, and normalized interfacial and frontal areas of the drop can vary non-monotonically with the Weber number, exhibiting as many as four local extrema. The results are compared to previous theoretical and experimental work, and implications for drop motion and heat and mass transfer are discussed.

1. Introduction

Flow internal and external to nearly spherical or deformed drops and bubbles is important in a number of applications, including liquid–liquid extraction and reaction (Weaver, Lapidus & Elgin 1959; Wellek, Agrawal & Skelland 1966; Brunson & Wellek 1970; Schügerl *et al.* 1977), cloud physics (Pruppacher & Beard 1970; Beard 1976; Pruppacher & Klett 1978), scavenging of particulate and trace gases by raindrops falling through the atmosphere (Walcek & Pruppacher 1984), direct contact heat

---

† Present address: Xerox Corporation, Wilson Center for Research and Technology, 800 Phillips Road, Webster, NY 14580, USA.

‡ Author to whom correspondence should be addressed.

transfer (Raina & Grover 1982), spray cooling (Mudawar & Deiters 1994), and spray combustion (Law 1982; Faeth 1983; Sirignano 1983, 1993; Dwyer 1989).

The effects of a solid boundary can be important in many cases. These include bubble flow in through-holes of printed circuit boards during electrodeposition of copper (Kilgore 1971), bubbling of air or other gases into chemical reactors (Crabtree & Bridgwater 1969; Nienow 1990), tertiary oil recovery (Payatakes 1982; Shyeh-Yung & Stadler 1995), gas sparging of power-plant cooling water discharge to reduce dissolved gas concentrations (Krabach *et al.* 1977), and two-phase flow in pipes (Hewitt & Hall-Taylor 1970; Maeda 1975; Dukler *et al.* 1988). In applications (e.g. modelling of steam generator tube rupture; cf. Kalra 1990), wall corrections to drag and terminal velocity are typically based on empirical correlations (e.g. Harmathy 1960).

Early analytical work (Hadamard 1911; Rybczynski 1911) considered Stokes flow of a dispersed phase moving with little or no deformation through an unbounded continuous phase. Saito (1913) showed that no deformation of the drop occurs at zero Reynolds number. This work has been summarized by Taylor & Acrivos (1964), who correctly extended the analysis to account for deformation at small non-zero Reynolds number. Haberman & Sayre (1958) calculated Stokes flow in and around an undeformed drop in a tube, either moving with constant velocity due to an axial body force (e.g. gravity in a vertical tube) in an otherwise quiescent fluid, or levitated in place against the body force by drag due to an upward (pressure gradient-driven) Poiseuille flow. They used linear superposition to study flow driven by a combination of body force and pressure gradient. This problem was later considered by Hetsroni, Haber & Wacholder (1970), who discussed the relationship between deformation and interfacial stress, and drop migration towards and away from the tube axis. Other theoretical studies of creeping flow of undeformed spherical drops in circular tubes have been reviewed by Happel & Brenner (1965), Clift, Grace & Weber (1978), and Grace (1983). Among these, Brenner (1971) showed that if the ratio of drop radius to tube radius is very small and the ratio of drop viscosity to that of the suspending liquid does not exceed 0.48, then the drop will flow at the same bulk velocity with a smaller pressure gradient than required for the same volumetric flow of the suspending liquid alone. By means of a boundary integral method, Martinez & Udell (1990) considered axisymmetric creeping flow of a neutrally buoyant deformable drop in a tube, and found that drop shape and speed became insensitive to drop size if the radius of an undeformed drop of equal volume exceeded the tube radius by 10% or more. To our knowledge, these and all other theoretical and computational treatments of deformable drop motion in a tube (Ho & Leal 1975; Coutanceau & Thizon 1981; Chen, Dagan & Maldarelli 1991; Pozrikidis 1992) have been restricted to Stokes flow. (We note that the work of Sheth & Pozrikidis (1995) pertains to two-dimensional flow in a spanwise infinite channel.)

Computations of steady axisymmetric deformable drop motion at non-zero Reynolds number have been limited to unbounded flows. A preliminary finite-element computation was presented by Tsukada *et al.* (1984) for the body force-driven case. Dandy & Leal (1989) conducted a more extensive investigation of the same problem using a finite-difference method. Among other results, they found that for Reynolds numbers 60 and 100 (based on drop diameter and viscosity of the suspending fluid) and for several combinations of the Weber number, viscosity ratio, and density ratio, the wake behind an axisymmetric drop includes a disjoint, closed recirculation zone, previously seen in the undeformed drop computations of Rivkind & Ryskin (1976). This zone has no counterpart in the wake of a bubble, a solid sphere, or in the creeping flow limit for a drop. To our best knowledge, a disjoint recirculation zone in the wake of a drop has not been observed experimentally† and it is not clear whether such flows are physically realizable (i.e. stable, and reachable from some initial condition).

According to Clift *et al.* (1978; p. 233), wall effects on drop motion will be significant (for Reynolds numbers less than 600, defined as before) if the ratio of the diameter of an undeformed drop with equivalent volume to the diameter of the tube is greater than 0.13. They note that previous correlations of experimental data are either limited to specific systems, failed to recognize the different regimes of fluid particles, or are difficult to apply. Other work includes measurements by Haberman & Sayre (1958) of drag coefficients and eccentricities of aqueous glycerine drops and silicone oil drops falling through castor oil (maximum Reynolds number 0.72, based on drop diameter and castor oil viscosity), experimental studies by O'Brien (1969) of drops whose undeformed radii exceeded the tube radius and wetted the wall, and experimental work of Ho & Leal (1975) and Olbricht & Leal (1982) on creeping circular Poiseuille flow (maximum Reynolds number about 0.25, based on bulk velocity, tube radius, and viscosity of the suspending liquid) with drops having radii comparable to that of the tube.

In this paper, we consider steady axisymmetric flow due to a deformable drop falling or rising at non-zero Reynolds number along the axis of a vertical tube under the action of gravity. In §2, we present the equations governing this free-boundary problem and describe the Galerkin finite-element technique used to approximate their solution. In §3, we present detailed numerical results. A discussion follows in §4.

2. Formulation and computational technique

2.1. *Formulation*

We consider axisymmetric flow of a liquid drop of volume $\frac{4}{3}\pi R_d^3$ and density ρ_d moving at constant velocity U through an immiscible, otherwise quiescent suspending fluid of density ρ_s in a tube of radius R_t. Motion is driven by gravity or another uniform body force aligned with the tube axis. The two fluids are taken to be Newtonian and incompressible. Although the numerical results in §3 will be restricted to the case in which the two fluids have the same dynamic viscosity, we will, for the sake of generality in the formulation, retain different viscosities, denoted by μ_d and μ_s, in the drop and suspending fluid, respectively. The interfacial tension, σ, between the fluids is taken to be constant. We select a reference frame moving with the drop, and locate the origin of an (r, z)-coordinate system at the centre of mass of the drop (figure 1).

The variables and equations that follow are rendered dimensionless by choosing R_t and U as the characteristic length and velocity, respectively. Subscripts d and s appended to field variables denote quantities associated with the drop and suspending fluid, respectively.

In each phase, flow is governed by the steady incompressible Navier–Stokes equations, internal

$$\frac{\rho_d}{\rho_s}\frac{R_t}{R_d}\frac{Re}{2}\boldsymbol{u}_d\cdot\nabla\boldsymbol{u}_d = \nabla\cdot\boldsymbol{T}_d, \tag{1a}$$

$$\nabla\cdot\boldsymbol{u}_d = 0, \tag{1b}$$

---

† Unlike Rivkind & Ryskin (1976, p. 8) and Dandy & Leal (1989, p. 162), we find no mention of this feature in Garner & Tayeban (1960*a*, *b*) and note that the work described in the dissertation of Le Clair (1970) is exclusively computational.

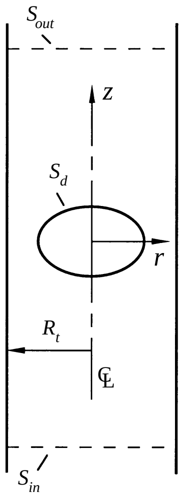

FIGURE 1. Definition sketch.

and external
$$\frac{R_t}{R_d}\frac{Re}{2}\boldsymbol{u}_s\cdot\nabla\boldsymbol{u}_s=\nabla\cdot\boldsymbol{T}_s, \tag{2a}$$

$$\nabla\cdot\boldsymbol{u}_s=0, \tag{2b}$$

to the drop. Here, the Reynolds number $Re = 2\rho_s R_d U/\mu_s$ is based on the properties of the suspending fluid and the undeformed drop radius. The stress tensors take the forms

$$\boldsymbol{T}_d=-\Pi_d\boldsymbol{I}+\frac{\mu_d}{\mu_s}[\nabla\boldsymbol{u}_d+(\nabla\boldsymbol{u}_d)^T] \tag{3a}$$

and
$$\boldsymbol{T}_s=-\Pi_s\boldsymbol{I}+[\nabla\boldsymbol{u}_s+(\nabla\boldsymbol{u}_s)^T], \tag{3b}$$

where $\Pi_j = (p_j-\rho_j gz)/(\mu_s U/R_t)$ $(j = d,s)$ is the dimensionless pressure in phase j, and $\boldsymbol{I}$ is the identity tensor. The stress and pressure are measured in units of $\mu_s U/R_t$. In cylindrical coordinates, the axisymmetric swirl-free velocity fields $\boldsymbol{u}_d$ and $\boldsymbol{u}_s$ have components $(u_d, 0, w_d)$ and $(u_s, 0, w_s)$, respectively, in the r-, ϕ-, and z-directions.

At the fluid–fluid interface, conservation of momentum is expressed by the traction boundary condition

$$\boldsymbol{n}\cdot(\boldsymbol{T}_s-\boldsymbol{T}_d)=\frac{1}{Ca}\left[\frac{\mathrm{d}\boldsymbol{t}}{\mathrm{d}s}+\frac{\boldsymbol{n}}{r}\frac{\mathrm{d}z}{\mathrm{d}s}\right]-\boldsymbol{n}St\left(\frac{R_t}{R_d}\right)^2 z, \tag{4}$$

on the surface S_d. Here, $Ca = \mu_s U/\sigma$ is the capillary number, $St = (\rho_d-\rho_s)gR_d^2/(\mu_s U)$ is a dimensionless buoyancy force, $\boldsymbol{n}$ and $\boldsymbol{t}$ are the local unit normal and tangent vectors to the interface, and s is the arclength along the interface measured from the forward stagnation point. We take $\boldsymbol{n}$ to be directed into the drop and $\boldsymbol{t}$ to be in the direction of increasing s, so that the second factor of the first term on the right-hand side of (4) is the sum of the local mean curvatures. The interface is a material surface, provided no mass transfer occurs across it; its shape is unknown *a priori*. For steady flow, the kinematic conditions at the drop interface S_d are

$$\boldsymbol{n}\cdot\boldsymbol{u}_d=0,\quad \boldsymbol{n}\cdot\boldsymbol{u}_s=0. \tag{5a, b}$$

On this surface, the velocity is continuous

$$\boldsymbol{u}_s=\boldsymbol{u}_d. \tag{6}$$

At the tube wall ($r = 1$), the suspending fluid moves relative to the drop and satisfies the no-slip and no-penetration conditions, namely,

$$\boldsymbol{u}_s = \boldsymbol{e}_z, \tag{7}$$

where $\boldsymbol{e}_z$ is the unit vector in the z-direction. The velocity asymptotically approaches a uniform flow

$$\boldsymbol{u}_s \rightarrow \boldsymbol{e}_z, \tag{8}$$

as $|z| \rightarrow \infty$.

Along the axis of symmetry ($r = 0$), we impose the conditions

$$\boldsymbol{e}_z \boldsymbol{e}_r : \boldsymbol{T}_s = 0, \quad u_s = 0, \quad \boldsymbol{e}_z \boldsymbol{e}_r : \boldsymbol{T}_d = 0, \quad u_d = 0, \tag{9a–d}$$

where $\boldsymbol{e}_r$ is the unit vector in the r-direction.

Equations (1)–(9) involve the dimensionless parameters Re, Ca, R_d/R_t, ρ_d/ρ_s, μ_d/μ_s, and St. Specification of any five fixes the sixth. Thus, the geometry, fluid properties, and acceleration due to gravity determine the terminal velocity of the drop, and hence Re and Ca. Alternatively, if the terminal velocity, geometry, and fluid properties are specified, then the buoyancy force must balance the drag on the drop, and g is thus determined. For the present problem, it is convenient to specify Re, Ca, R_d/R_t, ρ_d/ρ_s, and μ_d/μ_s, and to require that the drop centre-of-mass remains at the origin

$$z_{cm} = \iiint_V z \, \mathrm{d}V = \int_{S_d} z \, \pi r^2 \frac{\mathrm{d}z}{\mathrm{d}s} \mathrm{d}s = 0. \tag{10}$$

Thus, St is an unknown determined as part of the solution.

2.2. *Computational method*

The free-boundary problem (1)–(10) is solved on the domain including the deformable interface separating the drop and the suspending fluid, using a Galerkin finite-element method implemented in a modification of a code developed by Scriven and coworkers (Kistler & Scriven 1983; Christodoulou & Scriven 1989; Christodoulou 1990; de Santos 1991).

The domain is subdivided into a set of quadrilateral elements (cf. Strang & Fix 1973), each of which is mapped onto a unit square. On each unit square, the unknown velocity and pressure fields are represented by an expansion in biquadratic and linear basis functions, respectively. That is, the discretization is performed in the mixed interpolation sense (Huyakorn *et al.* 1978) to avoid over-constraint problems. To facilitate simultaneous determination of the flow and interface shape, an elliptic mesh generation scheme (Thompson, Warsi & Mastin 1985) developed by Christodoulou & Scriven (1992) and modified by de Santos (1991) is employed. The essence of the method is to determine the locations of the nodal or mesh points of a finite-element grid by solving a pair of elliptic partial differential equations

$$\boldsymbol{\nabla} \cdot D_\xi \boldsymbol{\nabla} \xi = 0, \quad \boldsymbol{\nabla} \cdot D_\eta \boldsymbol{\nabla} \eta = 0, \tag{11a, b}$$

where the 'diffusion' coefficients D_ξ and D_η are adjustable functions of position prescribed to meet particular requirements for the distribution of nodal or mesh points in the domain. The computational burden of solving the mesh generation equations (11a, b) is reduced by using the subparametric nodal position mapping described by Christodoulou & Scriven (1992), instead of the isoparametric mapping commonly used in finite-element computations. The mesh is determined concomitantly with the flow (see below), allowing the 'origin' of the finite-element mesh to vary relative to the centre-of-mass.

Inflow and outflow boundary conditions replacing (8) are imposed a finite distance upstream and downstream of the drop. At the inflow boundary S_{in}, a Dirichlet condition analogous to (8) is specified for $0 \leqslant r \leqslant 1$. At the outflow boundary S_{out}, the Neumann and Dirichlet conditions

$$\boldsymbol{nn}\colon \nabla \boldsymbol{u}_s = 0, \quad \boldsymbol{t}\cdot\boldsymbol{u}_s = 0, \quad \Pi = 0, \tag{12a–c}$$

are imposed on the z- and r-components of velocity, and the pressure.

To eliminate variations in drop volume associated with discretization and other sources of numerical error, we also impose a volume constraint

$$\int_{S_d} \pi r^2 \frac{\mathrm{d}z}{\mathrm{d}s}\,\mathrm{d}s = \tfrac{4}{3}\pi (R_d/R_t)^3, \tag{13}$$

which requires an additional degree of freedom in the mathematical system. This is obtained by specifying a reference pressure, independent of (12c), at a point inside the drop. Since specifying the pressure at any node in the domain determines (through the partial differential equations and boundary conditions) the pressure reference, specifying the pressure independently inside and outside the drop requires introduction of an undetermined 'correction factor' $\Delta\Pi_0$ to the pressure jump across the drop interface. Numerically, this is accomplished by replacing one of the discretized field equations at one point in the drop by an essential condition for pressure, and by introducing the additive term $\Delta\Pi_0$ in the normal stress boundary condition. The net effect is to add one equation (13) and one additional unknown ($\Delta\Pi_0$), leaving the system well-posed.

The Galerkin finite-element statement of the problem is completed by imposing boundary conditions on the mesh generation equations (11a, b). Along the drop interface and boundaries parallel to it in the computational domain, equal arclength spacing of grid points is enforced by Dirichlet conditions on the relevant mesh generation equations. On boundaries perpendicular to the interface in the computational domain, Dirichlet conditions are imposed with non-uniform D_ξ or D_η defined in a piecewise fashion (Eiseman 1982a, b; Thompson, Warsi & Mastin 1982, 1985; de Santos 1991; Christodoulou & Scriven 1992), so that grid points are compressed toward the interface where additional resolution is anticipated to be most useful.

Once the mathematical system is completely described, the nodal values and nodal locations are represented in the mixed interpolation scheme

$$\boldsymbol{u} = \sum \boldsymbol{u}_i \phi^i(\xi,\eta), \tag{14}$$

$$\Pi = \sum \Pi_k \Psi^k(\xi,\eta), \tag{15}$$

$$\boldsymbol{x} = \sum \boldsymbol{x}_l \theta^l(\xi,\eta). \tag{16}$$

Here, ϕ^i and Ψ^k are the biquadratic and linear discontinuous basis functions in the (ξ,η) domain, respectively, $\boldsymbol{x}_l$ are the nodal locations, and θ^l is the subparametric mapping function (cf. Christodoulou & Scriven 1992). Galerkin's method is applied by weighting the governing equations (1a, 2a) with ϕ^i, (1b, 2b) with Ψ^k, and (11a, b) with θ^l. The weighted equations are then integrated over the entire physical domain to obtain

$$\boldsymbol{R}_i^M \equiv \int_A [(B\boldsymbol{u}\cdot\nabla\boldsymbol{u})\phi^i + \nabla\phi^i\cdot\boldsymbol{T}]\,\mathrm{d}A - \int_{\partial A} \boldsymbol{n}\cdot\boldsymbol{T}\phi^i\,\mathrm{d}s = \boldsymbol{0}, \tag{17}$$

$$R_k^C \equiv \int_A \Psi^k \nabla\cdot\boldsymbol{u}\,\mathrm{d}A = 0, \tag{18}$$

$$R_l^{G,\xi} \equiv \int_A \nabla\theta^l\cdot(D_\xi\nabla\xi)\,\mathrm{d}A - \int_{\partial A} \boldsymbol{n}\cdot(D_\xi\nabla\xi)\,\theta^l\,\mathrm{d}s = 0, \tag{19a}$$

$$R_l^{G,\eta} \equiv \int_A \nabla\theta^l \cdot (D_\eta \nabla\eta)\,\mathrm{d}A - \int_{\partial A} \boldsymbol{n}\cdot(D_\eta \nabla\eta)\,\theta^l\,\mathrm{d}s = 0, \qquad (19b)$$

for the residuals, where B is the 'phase-dependent' coefficient of the nonlinear term in (1*a*) or (2*a*), and superscripts M, C, and G refer to momentum, continuity, and mesh generation, respectively. Dirichlet conditions are prescribed by replacing the appropriate residual equation with an essential boundary condition (cf. Kistler & Scriven 1983). Neumann boundary conditions are enforced through the surface integrals in (17) and (19*a*, *b*). We form residuals for the position constraint (10)

$$R^F \equiv \int_{S_d} z\pi r^2 \frac{\mathrm{d}z}{\mathrm{d}s}\,\mathrm{d}s = 0, \qquad (20)$$

and volume constraint (13)

$$R^V \equiv \int_{S_d} \pi r^2 \frac{\mathrm{d}z}{\mathrm{d}s}\,\mathrm{d}s - \tfrac{4}{3}\pi(R_d/R_t)^3 = 0. \qquad (21)$$

Equation (17) symbolically represents two equations for each node throughout the domain, A, while (18) and (19) each represent a single equation for each node, and (20) and (21) are single equations. The divergence theorem was used to lower the order of derivatives in the discretized momentum and mesh generation equations. The system (17)–(21) constitutes a finite set of nonlinear algebraic equations which can be written in summary form as

$$\boldsymbol{R}(\{z_i\},\{r_i\},\{u_i\},\{w_i\},\{\Pi_i\},St,\Delta\Pi_0) = \boldsymbol{R}(\boldsymbol{q}) = \boldsymbol{0}. \qquad (22)$$

Here, $\{z_i\}$ and $\{r_i\}$ are the nodal position unknowns determined by the elliptic mesh generation equations (11*a*, *b*), $\{u_i\}$ and $\{w_i\}$ are the nodal values of the r- and z-components of velocity, and $\{\Pi_i\}$ are the nodal values of pressure. The vector $\boldsymbol{q}$ includes all nodal unknowns, in addition to St and $\Delta\Pi_0$. The system (22) is solved by Newton's method

$$\boldsymbol{J}^{(k)}\Delta\boldsymbol{q}^{(k+1)} = -\boldsymbol{R}^{(k)}. \qquad (23)$$

In (23), $\boldsymbol{J} = \partial\boldsymbol{R}/\partial\boldsymbol{q}$ is the Jacobian matrix of partial derivatives, $\Delta\boldsymbol{q}^{(k+1)} = \boldsymbol{q}^{(k+1)} - \boldsymbol{q}^{(k)}$, and k denotes the kth iterate. At each Newton iteration, the linear system (23) is solved by direct factorization or LU-decomposition of the Jacobian using a modification of Hood's frontal solver (Hood 1976; Walters 1980).

Critical to Newton's method is a sufficiently accurate initial iterate. A convenient initial iterate is obtained by solving the governing equations for Stokes flow ($Re = 0$) and small capillary number, e.g. $Ca = 0.005$ (equivalently, high interfacial tension), for which the drop shape is well-approximated by a sphere. Thereafter, steady solution families are traced efficiently by first-order continuation (Riks 1972; Keller 1977) either in Re, holding Ca fixed, or in Ca, holding Re fixed.

Inlet and outlet boundaries are located at $z = -5$ and $z = 10$, so that imposition of boundary conditions (8) and (12) a finite distance from the drop has virtually no effect on the solutions. Figure 2(*a*, *b*) shows a typical mesh of 760 elements. (Except where otherwise stated, this is the number used for results presented in this paper.) For each such mesh, the number of velocity, pressure, and nodal position unknowns is 6378, 2280 and 3189, respectively, and the interface is discretized into 40 adjacent segments, each corresponding to the common edge of one element in the drop and one outside, giving 81 interfacial nodes. For the meshes used, as typified by those shown in figure 2, elements at the origin appear triangular, and are implemented in our code as regular quadrilateral elements, for which two adjacent vertices coincide in the physical domain. Typically, five Newton iterations suffice to bring the L_2 norm of the residuals and the

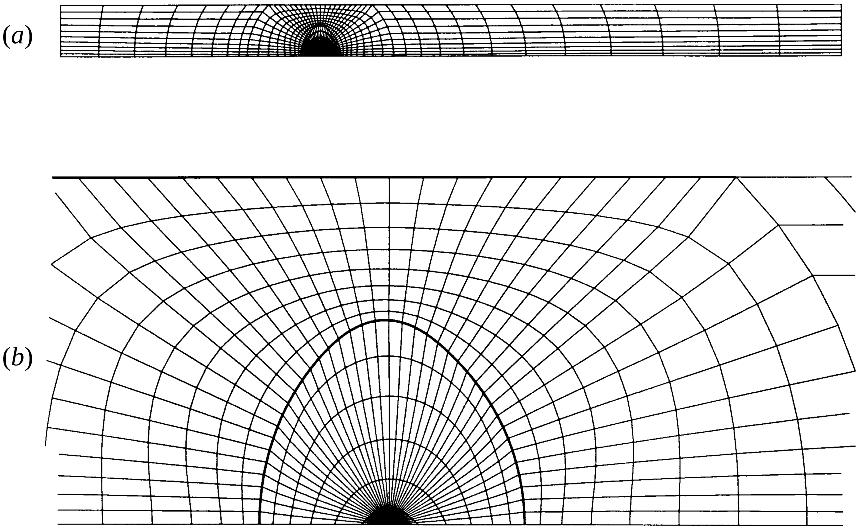

FIGURE 2. Typical finite-element mesh of problem domain produced by the elliptic mesh generator, with the interface shown in bold: (*a*) view of entire domain; (*b*) detail in and near drop.

error in the solution below 10^{-5}. For typical cases, decreasing the computational domain by 25 % in each direction along the z-axis has the effect of changing the length of the separated flow region by less than one part in 500, and affecting the drag coefficient, drop interfacial area, and other parameters discussed below by less than 0.01 %. Decreasing the number of elements in the tesselation by 200 changes the drag coefficient by less than 1 % for $Ca = 0.01$ and $Re = 240$. For the results presented here, Newton iteration always converged, with no hint of singularity in the Jacobian.

The code was validated by comparison to previous work, including the classic experimental work of Winnikow & Chao (1966) and the computational work of Dandy & Leal (1989), both in an unbounded domain, and Stokes flow calculations of Haberman & Sayre (1958) and Coutanceau & Thizon (1981) for an undeformed drop falling in a vertical tube. Winnikow & Chao (1966) obtained data for several rigorously purified liquid pairs. For comparison to our computations, we have chosen their results for 0.2 cm diameter bromobenzene drops in water, for which the viscosity ratio is closer to unity than the other liquid pairs they studied, and for which the Reynolds number is at the high end of the range considered in §3. We used the values of surface tension, terminal velocity, and bromobenzene dynamic viscosity reported by Winnikow & Chao (1966) and Winnikow (1965), along with the reported Re (539) to find the kinematic viscosity of water, from which we obtained the temperature (23.1 °C), and hence the dynamic viscosity and density of water. From these data, we calculate $Ca = 0.00602$. For $R_d/R_t = 0.1$ (corresponding to 1 % blockage), our computations (with 727 elements) give a drag coefficient of $C_D = 0.196$, and show that the drop is oblate with an axis ratio of 1.20, where we define the drag coefficient as

$$C_D = \frac{\frac{4}{3}\pi R_d^3 |\rho_s - \rho_d| g}{\frac{1}{2}\rho_s U^2 \pi R_d^2} = \frac{16 St}{3 Re}, \tag{24}$$

and the axis ratio as

$$\alpha = \frac{2 r_{max}}{\Delta z_{max}}, \tag{25}$$

where r_{max} and Δz_{max} are the maximum radial and axial extents of the drop, respectively. (Note that C_D is defined in terms of the frontal area of an undeformed drop of equal volume.) The excellent agreement with the corresponding experimental values of 0.201 and 1.22 reported by Winnikow & Chao (1966), for drops at high *Re* and with significant deformation, validates the code and also underscores the importance of rigorous fluid purification in experiments (see §4.1).

We have also compared our results to those of Dandy & Leal (1989) for $\rho_d/\rho_s = 0.91$, $\mu_d/\mu_s = 1.33$, and two different pairs of *Ca* and *Re* ($Ca = 0.2$, $Re = 5$; $Ca = 1$, $Re = 0.5$). For $R_d/R_t = 0.1$ and 0.2 (corresponding to 1 % blockage and 727 elements, and 4 % blockage and 742 elements, respectively), we compute $C_D = 6.24$ and 7.13, respectively (for $Ca = 0.2$ and $Re = 5$), and 50.9 and 64.05, respectively (for $Ca = 1$ and $Re = 0.5$), compared to corresponding values of 5.80 and 42.3 obtained by Dandy & Leal in the unbounded case. These results are consistent with physical intuition, in that our drag coefficients exceed those for the unbounded case, with the smaller fractional difference being for the higher *Re*, for which wall effects are expected to be less important. In addition, for $\rho_d/\rho_s = 0.91$, $\mu_d/\mu_s = 1.33$, $Re = 100$, $Ca = 0.04$, and $R_d/R_t = 0.1$, we obtain $C_D = 0.893$ (using 727 elements) compared to 0.919 reported by Dandy & Leal. This is not consistent with physical intuition. Hence, we successively reduced the number of elements in our computation to 547, 445 and 405. The computed values of C_D increased monotonically to 0.894, 0.897 and 0.901, respectively. Thus, we believe that for $\rho_d/\rho_s = 0.91$, $\mu_d/\mu_s = 1.33$, $Re = 100$, and $Ca = 0.04$, the drag coefficient with 1 % blockage does not exceed 0.893. From this, and our belief that the drag coefficient for the unbounded case should be lower, we conjecture that the small discrepancy is due to lack of grid convergence in the results of Dandy & Leal (1989).

Excellent comparison to the Stokes flow results of Haberman & Sayre (1958) and Coutanceau & Thizon (1981) is presented in §4.1.

3. Results

As described in §2.1, there are five independent dimensionless parameters, namely Re, Ca, R_d/R_t, ρ_d/ρ_s, and μ_d/μ_s. Here, we consider $\mu_d/\mu_s = 1$, $R_d/R_t = 0.5$, and $\rho_d/\rho_s = 6/5$ and $5/6$. Restriction to the homoviscous case $\mu_d/\mu_s = 1$ allows consideration of inertial, buoyancy, and interfacial tension effects absent the effects of viscosity contrast that occur for $\mu_d/\mu_s \neq 1$. This restriction has been discussed by Pozrikidis (1990, 1992), Sheth & Pozrikidis (1995), and Buckmaster & Flaherty (1973). Moreover, as pointed out by Buckmaster & Flaherty (1973), there is no reason to believe that the homoviscous case is atypical. This case has received relatively little attention from Dandy & Leal (1989) (see their figure 9 and table 1). The two density ratios were chosen to illustrate the similar behaviour displayed by falling and rising drops with ρ_d/ρ_s near unity. We henceforth refer to the suspending fluid as a liquid.

In what follows, we present drop shapes and streamlines as a function of Reynolds number for several capillary numbers, as well as 'integral' properties of the flow, including the 'normalized' interfacial area

$$A_{surface} = \frac{1}{4\pi(R_d/R_t)^2}\int_{S_d} 2\pi r \,\mathrm{d}s, \tag{26}$$

and frontal area

$$A_{frontal} = \frac{r_{max}^2}{(R_d/R_t)^2}. \tag{27}$$

The areas and axis ratio provide quantitative measures of drop shape. Although a

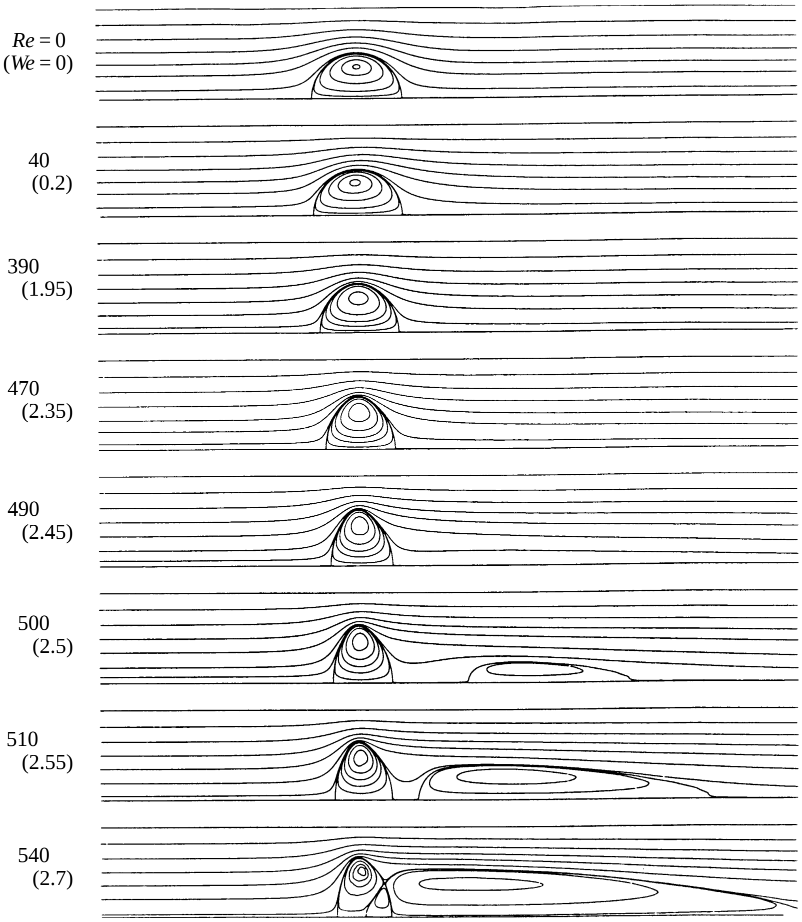

FIGURE 3. Streamlines and interface shapes for $Ca = 0.005$ and $\rho_d/\rho_s = 6/5$. Note that the external recirculation zone shown for $Re = 540$ falls well within the axial extent of the computational domain.

spherical drop necessarily has an axis ratio of unity, not all drops of unit axis ratio are spherical.

We group the results according to capillary number. Each group consists of results for two or more values of Ca, for each of which a sequence of flows was computed for increasing Re starting with a nearly spherical drop at or near $Re = 0$. As expected, at any Re, departures from sphericity became more pronounced as Ca increases. For each flow field shown, we also indicate the value of the Weber number $We = Re\,Ca$. The streamlines are level curves of $\mathrm{d}r/u = \mathrm{d}z/w$.

In §§3.1–3.3, we focus on the falling drop case, $\rho_d/\rho_s = 6/5$, and in §3.4 we briefly present results for $\rho_d/\rho_s = 5/6$.

3.1. *Falling drops*, $0.005 \leqslant Ca \leqslant 0.01$

We begin with $Ca = 0.005$ to illustrate the effects of high interfacial tension. Figure 3 shows streamline plots for $Re = 0$, 40, 390, 470, 490, 500, 510 and 540 detailing the development of the flow structure and drop deformation. The vertically downward drop motion is depicted as a left-to-right flow of the suspending liquid in the drop-fixed frame. At $Re = 0$, the drop shape is essentially spherical with the computed axis ratio differing from unity by less than one part in 10000. With increasing Re, the drop

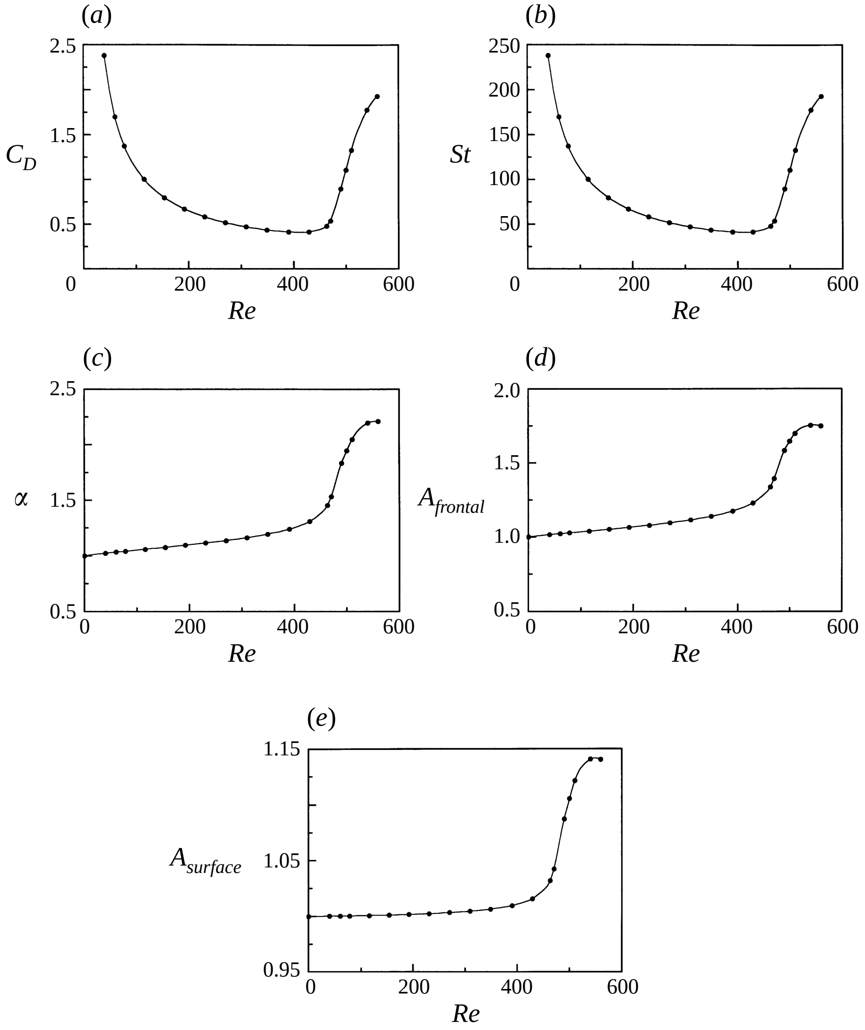

FIGURE 4. Variation of integral properties with Re for $Ca = 0.005$ and $\rho_d/\rho_s = 6/5$. (a) C_D; (b) St; (c) α; (d) $A_{frontal}$; (e) $A_{surface}$.

deforms oblately and becomes increasingly asymmetric, as shown for $Re = 40, 390, 470$ and 490. Although fore–aft asymmetry of the drop shape is not apparent from the plotted interface until $Re = 470$, the streamlines are clearly asymmetric by $Re = 40$. By $Re = 500$, a disjoint recirculation zone has developed in the drop wake, as noted in the unbounded case by Dandy & Leal (1989) for $\mu_d/\mu_s = 4$, $\rho_d/\rho_s = 0.91$, and several values of Re and Ca. As Re increases (see streamlines for $Re = 510$), the disjoint recirculation zone, with forward and rear stagnation points, has grown, intensified, and approached the drop from the rear. By $Re = 540$, it has attached to the drop and its forward stagnation point has crossed the drop interface. This crossing gives rise to three contiguous recirculation zones, two inside and one outside the drop, as shown for $Re = 540$, and discussed by Pruppacher & Beard (1970) and Rivkind & Ryskin (1976). The disjoint recirculation zone and its interaction with the drop are further discussed in §§3.2 and 4.2.

For $Ca = 0.005$, figures 4(a) and 4(b) show C_D and St, respectively, as functions of

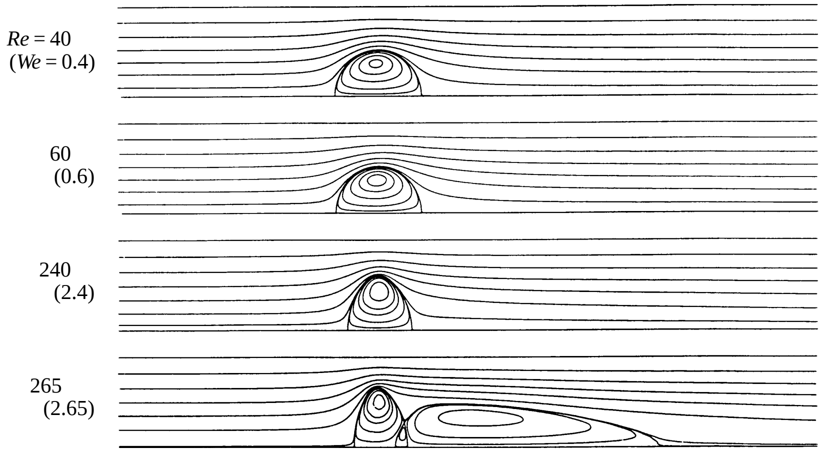

FIGURE 5. Streamlines and interface shapes for $Ca = 0.01$ and $\rho_d/\rho_s = 6/5$.

Re. In this and subsequent plots of integral properties *vs.* Re, filled-in circles indicate the values of selected computations. Other computed values, also lying on the curves, have been omitted for graphical clarity. In figure 4(*a*), we see that the plot of C_D *vs.* Re consists of decreasing and increasing segments. The transition in C_D near $Re = 460$ is due to the sharp increase in the axis ratio and frontal area of the highly oblate drop at this Re, as seen for $Re = 490$, 500, 510 and 540. Figure 4(*b*) shows that St increases monotonically, with a change in slope near $Re = 460$. For $Re \leqslant 460$, St is nearly independent of Re, as indicated by (24) and the nearly inverse relationship between C_D and Re shown in figure 4(*a*). For $Re \geqslant 460$, C_D increases rapidly with Re, corresponding to a significantly increased slope of the St *vs.* Re plot, at least for $Re \leqslant 540$. Figures 4(*c*)–4(*e*) show the geometric measures α, $A_{frontal}$, and $A_{surface}$, respectively, as functions of Re. For the present parameter values, these quantities depend similarly on Re, also exhibiting a change of slope near $Re = 460$. Development of the trailing recirculation zone is clearly associated with the oblateness of the drop near $Re = 500$, for which $\alpha \approx 1.8$ and $A_{frontal} \approx 1.6$, as shown in figures 4(*c*) and 4(*d*). We note that the increase in C_D occurs at an Re slightly smaller than that at which the recirculation zone first appears. Thus, unlike the rigid-sphere case, development of the recirculation zone is immediately followed by a transition from $\mathrm{d}C_D/\mathrm{d}(Re) < 0$ to $\mathrm{d}C_D/\mathrm{d}(Re) > 0$.

Increasing Ca corresponds to decreasing the interfacial tension, and hence to greater drop deformation. Thus, for $Ca = 0.01$ the computed flows show more deformation at a given Re than for $Ca = 0.005$, but are quite similar to those found at higher Re for $Ca = 0.005$. (Presentation of results for larger Ca will be limited to those for which noteworthy features appear.) At $Ca = 0.01$, as shown in figure 5, drop deformation is evident at values of Re below which the $Ca = 0.005$ drop is essentially spherical. For $Ca = 0.01$, noticeable departure from sphericity ($\alpha = 1.07$) occurs near $Re = 60$, while for $Ca = 0.005$ comparable deformation ($\alpha = 1.08$) is not apparent until $Re = 154$ (not shown). Results for $Ca = 0.005$ and $Re = 490$ (figure 3) are qualitatively similar to those for $Ca = 0.01$ and $Re = 240$. Development of a disjoint recirculation zone proceeds as for $Ca = 0.005$, with the forward stagnation point of the disjoint recirculation zone ultimately crossing the drop interface as shown for $Re = 265$. For $Ca = 0.01$, figure 6 shows that C_D *vs.* Re is very similar to the $Ca = 0.005$ case, if one rescales the abscissa according to $Re' = We = Re\,Ca$. Similar agreement obtains for the other integral measures (α, $A_{frontal}$, and $A_{surface}$). By reference to figures 3–6, we

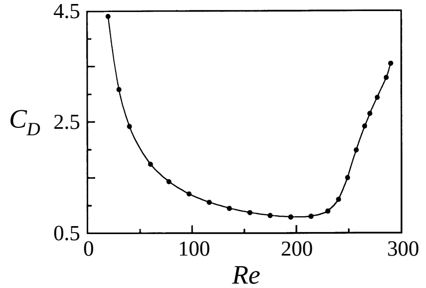

FIGURE 6. Variation of C_D with Re for $Ca = 0.01$ and $\rho_d/\rho_s = 6/5$.

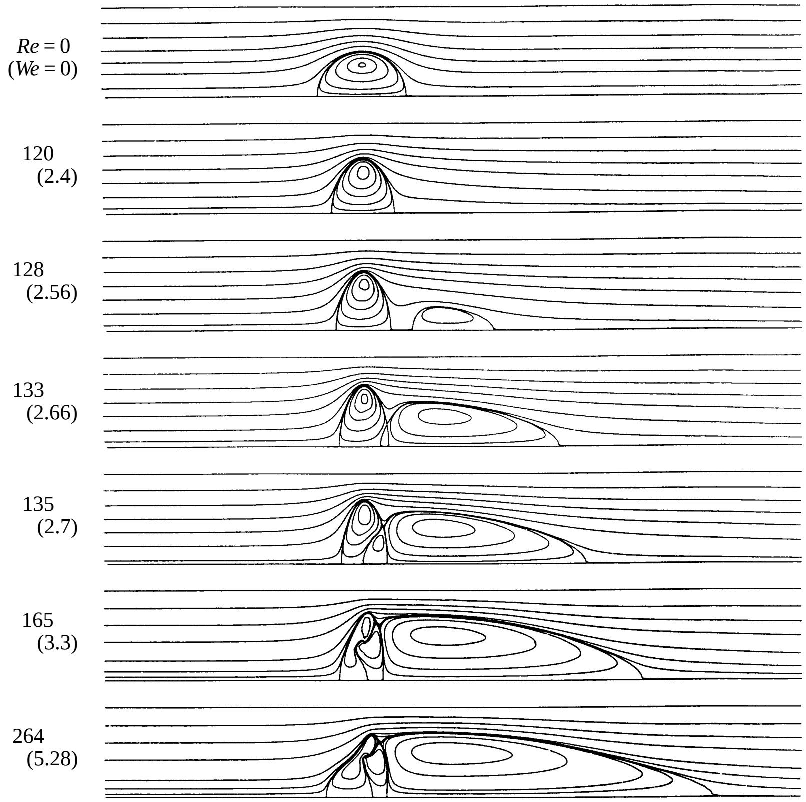

FIGURE 7. Streamlines and interface shapes for $Ca = 0.02$ and $\rho_d/\rho_s = 6/5$.

note that the locations of extrema of quantities related to drop shape, and indeed the flow itself, depend primarily on *We*, as discussed previously for large *Re* (Feng & Basaran 1994).

3.2. *Falling drops*, $0.02 \leqslant Ca \leqslant 0.5$

Figure 7 shows development of the flow field and drop shape for $Ca = 0.02$ as Re increases. At $Re = 0$ the drop is still essentially spherical ($\alpha = 0.9996$). (We note that at $Re = 0$, the nature of the deformation is determined by the wall, rather than by the criterion of Taylor & Acrivos (1964) which, for small *Re*, predicts $\alpha > 1$ in homoviscous flow with $\rho_d/\rho_s < 53.125$.) For $Re = 120$, the drop is significantly oblate with slight fore–aft asymmetry. By $Re = 128$, a disjoint recirculation zone has developed, as described in §3.1. Streamlines for $Re = 133$ and 135 show that the forward stagnation

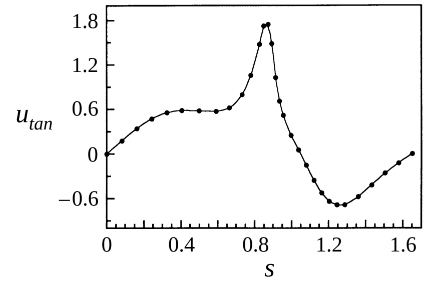

FIGURE 8. Variation of the interfacial tangential velocity component u_{tan} with arc-length s for $Ca = 0.02$, $\rho_a/\rho_s = 6/5$, and $Re = 264$. Other points, also lying on the curve, have been omitted for graphical clarity.

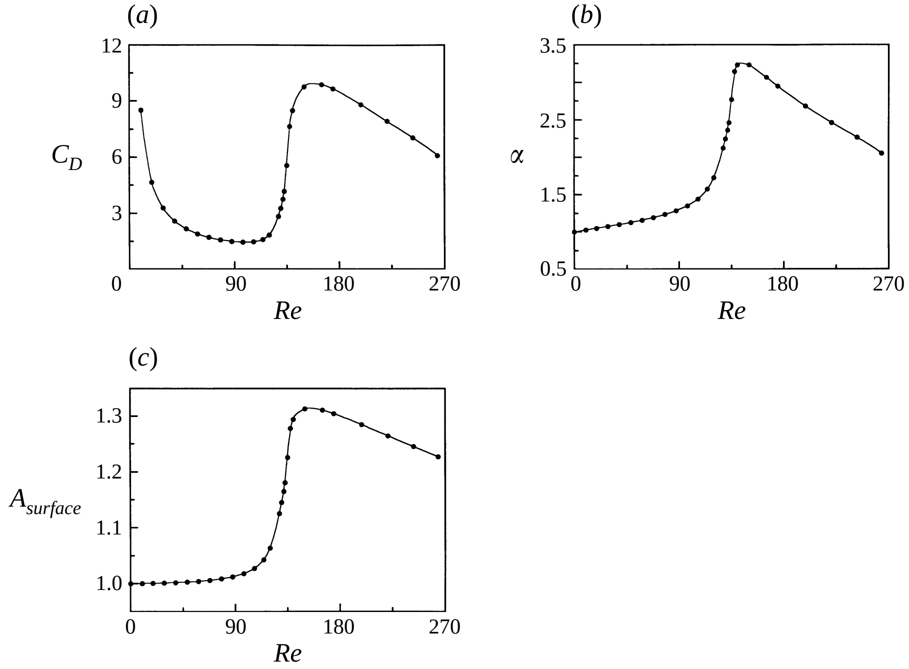

FIGURE 9. Variation of integral properties with Re for $Ca = 0.02$ and $\rho_a/\rho_s = 6/5$. (a) C_D; (b) α; (c) $A_{surface}$.

point of the separated flow region moves toward and eventually crosses the drop interface. By $Re = 135$, the drop has become more oblate ($\alpha = 2.77$) than those described in §3.1. Fore–aft asymmetry in the drop shape has become quite apparent by $Re = 165$. By $Re = 264$, an inflection circle has developed on the front of the drop, and the rear is no longer convex. For $Re = 264$, figure 8 shows the variation of the tangential velocity (u_{tan}) with arclength s along the drop surface (with the forward stagnation point at $s = 0$), passing through the separation circle on the rear of the drop where $u_{tan} = 0$ at $s \approx 1.05$ and ending at the rear stagnation point. We note, in particular, the rapid acceleration and deceleration that occur immediately fore and aft, respectively, of the tip of drop. To our knowledge, such 'hat-shaped' drops have not been observed previously.

Figures 9(a)–9(c) show C_D, α, and $A_{surface}$, respectively, as functions of Re for $Ca = 0.02$. As with the two series in §3.1, figure 9(a) shows that C_D decreases

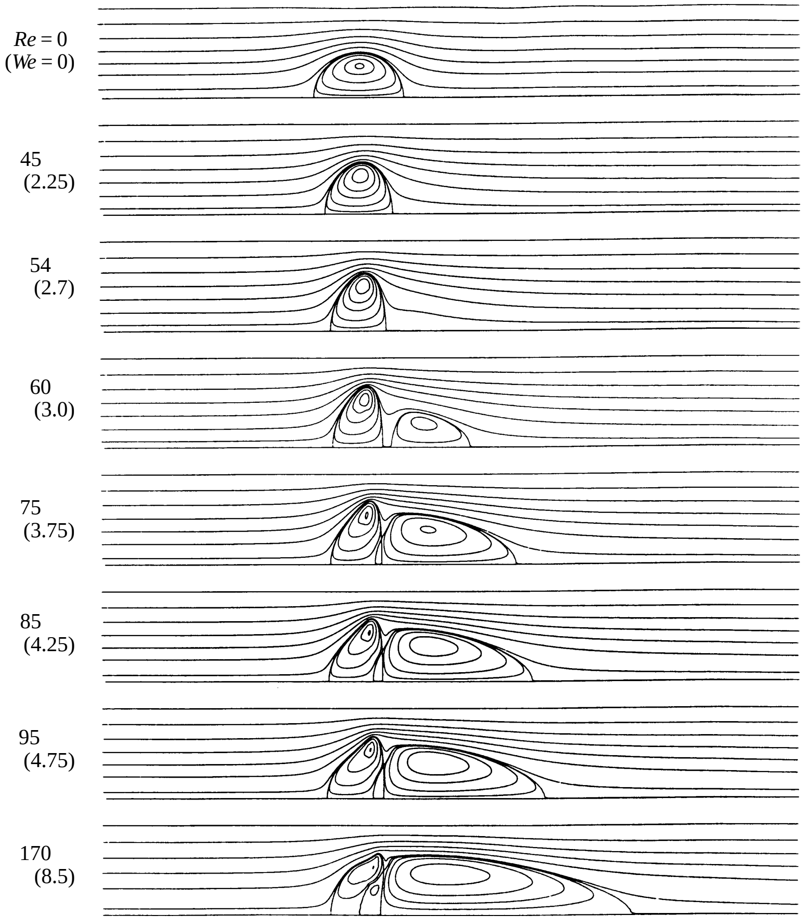

FIGURE 10. Streamlines and interface shapes for $Ca = 0.05$ and $\rho_a/\rho_s = 6/5$.

monotonically until $Re \approx 100$, and then increases sharply beginning at an Re slightly smaller than that at which development of a recirculation zone first becomes apparent. Between $Re = 121$ and 128, a recirculation zone appears. As Re increases past 160, C_D decreases once again. Figure 9(*b*) shows that α increases approximately linearly for Re up to about 90, and then increases much more rapidly until about $Re = 140$, beyond which it decreases nearly linearly up to at least $Re = 264$. The maximum value of α occurs at an Re slightly less than that at which the decrease of C_D at high Re shown in figure 9(*a*) begins. Although not apparent in figure 9(*b*), α passes through unity at a small non-zero Re, corresponding to transition from a prolate ($\alpha < 1$) to an oblate ($\alpha > 1$) drop. To the best of our knowledge, such non-monotonic behaviour of the axis ratio has not been reported previously. Variation of the interfacial area (figure 9*c*) follows a non-monotonic pattern similar to that noted for α.

For $Ca = 0.05$ (figure 10), drops are generally spherical for small Re, with α increasing from 0.9978 at $Re = 0$ to 1.07 at $Re = 10$ (not shown). Significant asphericity in drop shape and fore–aft asymmetry in the flow field become apparent by $Re = 45$. As Re increases, the drop stretches radially (cf. $Re = 54$), and the trailing surface begins to flatten. For $Re = 54$, we also note the appearance of a protuberance in the first streamline away from the axis. This feature precedes onset of a disjoint recirculation zone, which develops by $Re = 60$. The forward stagnation point of the

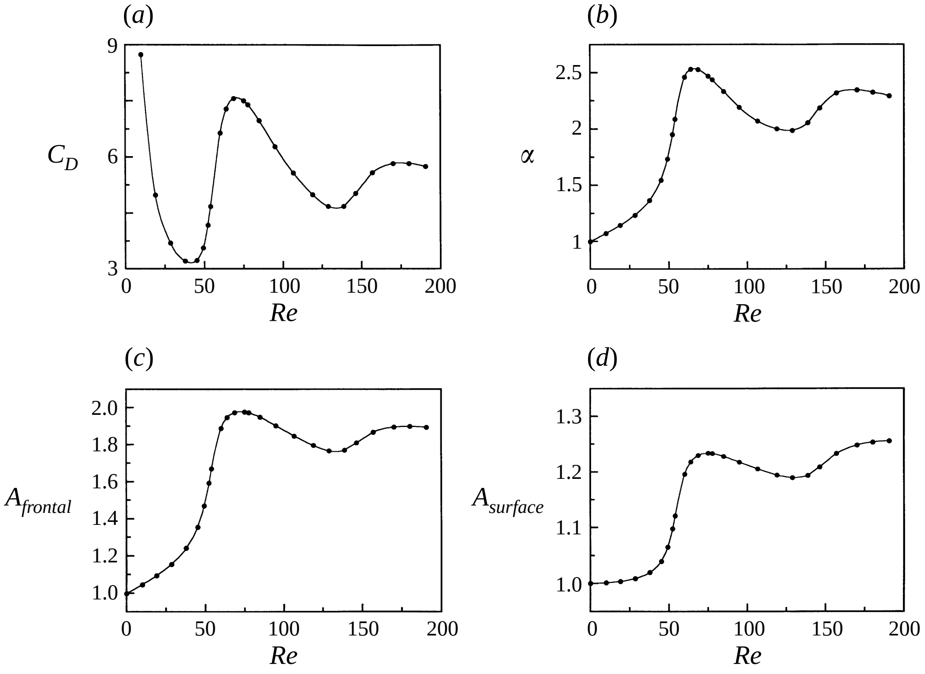

FIGURE 11. Variation of integral properties with Re for $Ca = 0.05$ and $\rho_d/\rho_s = 6/5$. (a) C_D; (b) α; (c) $A_{frontal}$; (d) $A_{surface}$.

disjoint recirculation zone crosses into the drop by $Re = 75$, and penetrates further into the drop by $Re = 85$. Near $Re = 95$, an inflection circle appears on the front of the drop interface, as for $Ca = 0.02$ ($Re = 264$). By $Re = 170$, the rear surface of the drop has lost its convexity.

Remarkable features are exhibited by the integral measures C_D, α, $A_{frontal}$, and $A_{surface}$, for $Ca = 0.05$, as shown in figures 11(*a*)–11(*d*). These integral measures vary non-monotonically with Re, with between two and four local extrema in the range of Re shown. In figure 11(*a*), we note a sharp transition from decreasing to increasing C_D at an Re near 40 and slightly smaller than that at which the recirculation zone is first apparent. Additional local extrema occur near $Re = 80$, 140 and 180. Figures 11(*b*)–11(*d*) show that α, $A_{frontal}$, and $A_{surface}$ have similar local extrema. Beyond $Re = 175$ the interfacial area, $A_{surface}$, continues to increase while the other quantities decrease (figure 11*d*). Re-examination of the results for $Ca = 0.005$, 0.02 and the present case shows that for $We = Re\,Ca < 2$, α increases nearly linearly with Re, and then increases with a much larger slope until about $We = 2.8$, beyond which it decreases. For $Ca = 0.05$, we see that another local minimum and maximum occur near $We = 6.3$ and 8.7, respectively. The amplitude of the oscillations in α and the other integral measures decreases with increasing Re.

For $Ca = 0.2$, figure 12 shows streamline plots for increasing Re. Here, the drop is clearly prolate ($\alpha = 0.97$) at $Re = 0$. As Re increases, the trailing surface of the drop flattens (cf. $Re = 10$) and eventually loses its convexity by $Re = 30$. Again (cf. $Re = 30$), a protruding streamline precedes appearance of the disjoint recirculation zone. By $Re = 50$, the drop appears crescent-shaped with round tips, and a disjoint recirculation zone has developed. At larger Re, the disjoint recirculation zone intensifies (cf. $Re = 60$), the tip of the crescent sharpens, and an inflection develops in the streamsurface dividing the external flow from the disjoint recirculation zone as the forward

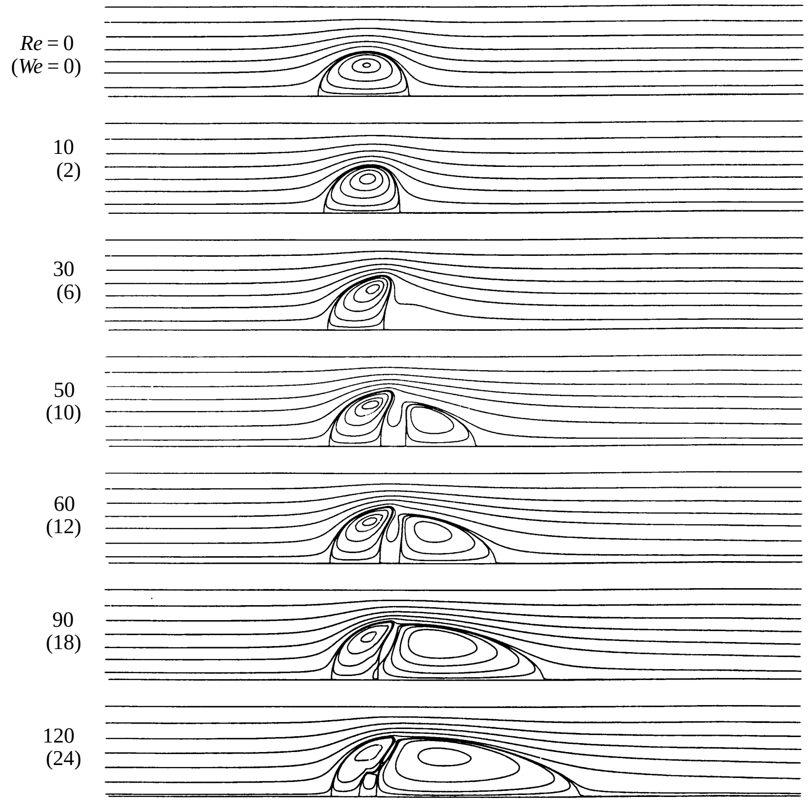

FIGURE 12. Streamlines and interface shapes for $Ca = 0.2$ and $\rho_d/\rho_s = 6/5$.

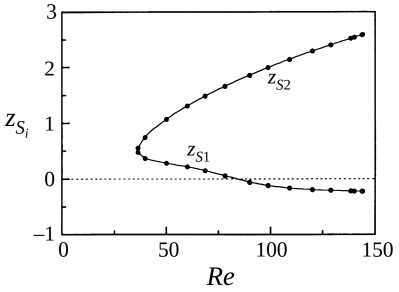

FIGURE 13. Positions of forward and rear stagnation points (z_{s1} and z_{s2}, respectively) of zone C vs. Re for $Ca = 0.2$ and $\rho_d/\rho_s = 6/5$.

stagnation point of the latter approaches and crosses the rear of the drop, as shown for $Re = 90$. By $Re = 120$, the rear recirculation zone in the drop has grown. We denote the forward and rear recirculation zones in the drop by A and B, respectively, while the recirculation zone in the suspending liquid will be referred to as C. The forward stagnation point of zone C moves toward the drop, crosses the drop interface, and subsequently becomes the forward stagnation point of zone B. For the present parameters, figure 13 illustrates this process by showing the rear stagnation point of zone C, denoted by z_{s2}, and the forward stagnation point of zone C (and after attachment and crossing, the forward stagnation point of zone B), denoted by z_{s1}, both defined relative to the rear of the drop. Note that $z_{s1} < 0$ indicates that the forward

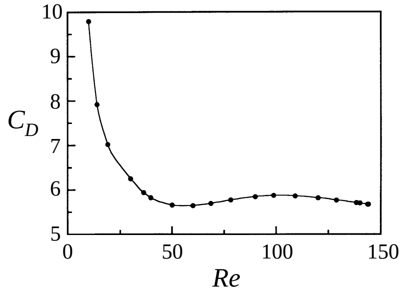

FIGURE 14. Variation of C_D with *Re* for $Ca = 0.2$ and $\rho_a/\rho_s = 6/5$.

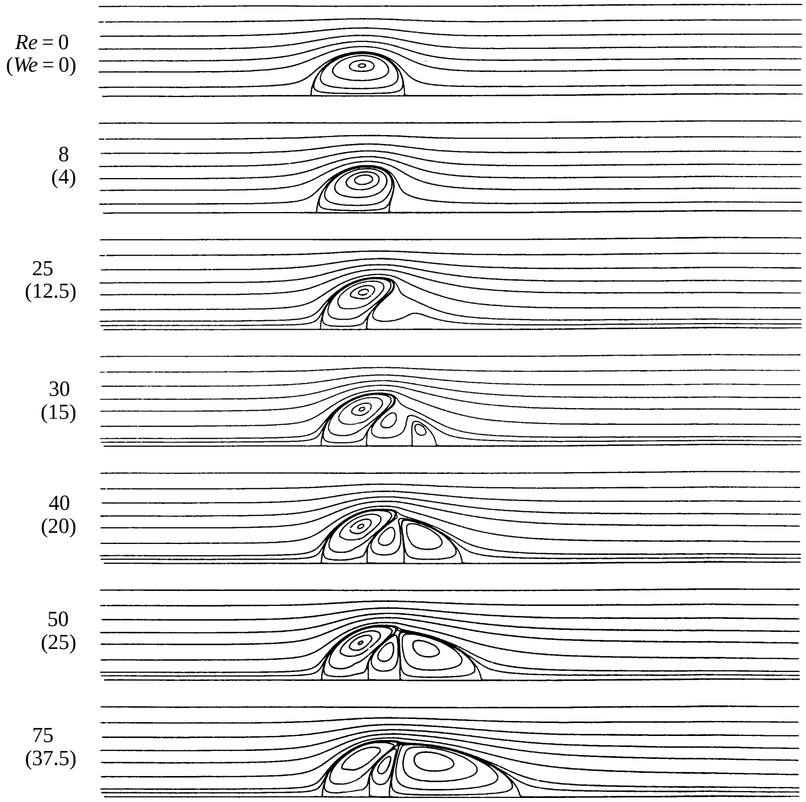

FIGURE 15. Streamlines and interface shapes for $Ca = 0.5$ and $\rho_a/\rho_s = 6/5$.

stagnation point of zone *C* has crossed the drop interface and now corresponds to the forward stagnation point of zone *B*. In figure 13, we see the appearance of a disjoint recirculation zone at $Re \approx 35$, at which z_{s1} and z_{s2} coincide, and note that the forward stagnation point of zone *C* first meets the drop interface at $Re \approx 85$. We further note that z_{s2} increases monotonically with *Re* until at least $Re = 145$, while z_{s1} decreases monotonically, passes through zero, and eventually reaches an apparent asymptote of approximately -0.23. Figure 14 shows that two shallow extrema persist in the C_D, *Re* plot.

Figure 15 shows streamlines for $Ca = 0.5$. At $Re = 0$, the drop is noticeably prolate ($\alpha = 0.93$). As *Re* increases, the drop becomes rear-indented (Fararoui & Kintner 1961; Pruppacher & Beard 1970; Baumann *et al.* 1989; Dandy & Leal 1989; Shopov

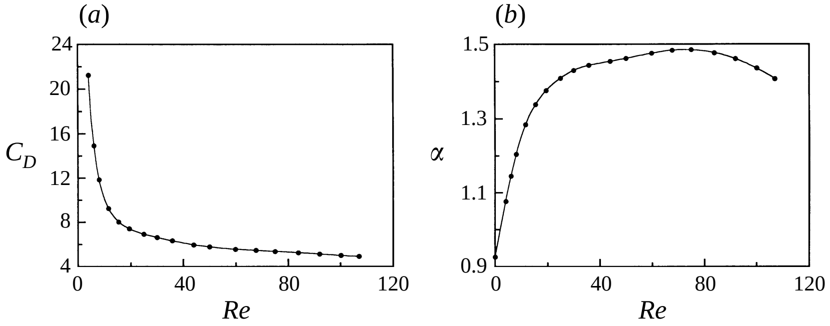

FIGURE 16. Variation of C_D and α with Re for $Ca = 0.5$ and $\rho_d/\rho_s = 6/5$. (a) C_D; (b) α.

& Minev 1992), thus losing its convexity ($Re = 8$), and becomes increasingly deformed, with its wing-tip swept back by the flow ($Re = 25$), resulting in a round-tipped crescent-shaped drop. By $Re = 30$, a disjoint recirculation zone has developed, but unlike previous cases, an additional external recirculation zone appears between the liquid–liquid interface and the rearmost recirculation zone (earlier described as zone C). Formation of this second recirculation zone external to the drop corresponds to 'pinching off' (closure) of a streamsurface exterior to the drop that follows the rear of the interface toward the symmetry axis, where it turns downstream, follows the axis rearward to the front of the disjoint recirculation zone, and then follows (initially radially outward and then to the rear) the streamsurface separating the primary (downstream) external recirculation zone from the bulk of the suspending liquid. At some Re, a streamsurface closes, and a second external recirculation zone forms. Note that these flows are qualitatively different from those shown in figure 12 for $Ca = 0.2$, in which case the streamsurfaces in the gap between the large external recirculation zone and the rear of the drop originate upstream of the drop and ultimately continue downstream (as shown in figure 12 for $Re = 60$). Thus, this gap is not a second external recirculation zone.

For $Re = 40$, 50 and 75, the disjoint recirculation zone is seen to move toward the drop. At $Re = 75$, we note that the drop is crescent-shaped and the drop and disjoint recirculation zone have developed a sharp tip and a near-90° corner, respectively, which nearly meet (graphical enlargement reveals that a small gap persists throughout the range of Re). Until at least $Re = 107$, the forward stagnation point of the disjoint recirculation zone does not cross the drop interface. Thus, although an external recirculation zone forms, as seen for previous cases, it remains disjoint well past values of Re for which it had previously attached to the drop.

Although the sequence of flows for $Ca = 0.5$ is quite striking, the corresponding plots of C_D and (figures 16*a* and 16*b*, respectively) are very similar to those obtained for $Ca = 0.2$. Figure 16(*a*) shows a rapid decrease in C_D until about $Re = 10$, beyond which it approaches a constant value of $C_D \approx 5$. The axis ratio increases until about $Re = 78$, beyond which it begins to decrease, as seen in figure 16(*b*). Figure 17 shows the forward and rear stagnation points of the disjoint recirculation zone as described for figure 13. Here, however, z_{s1} (again, defined relative to the rear of the drop) does not take on negative values, since the forward stagnation point of the disjoint recirculation zone does not cross the drop interface for $Re \leqslant 107$.

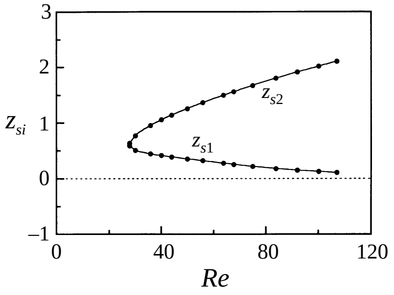

FIGURE 17. Positions of forward and rear stagnation points (z_{s1} and z_{s2}, respectively) of zone C vs. Re for $Ca = 0.5$ and $\rho_d/\rho_s = 6/5$.

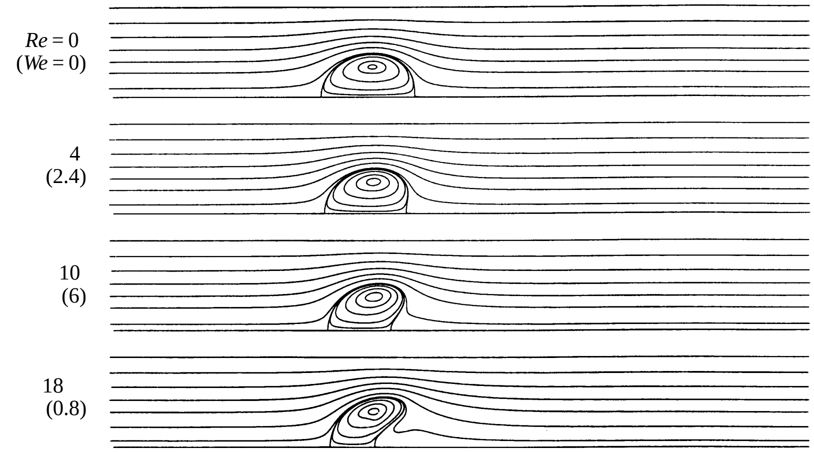

FIGURE 18. Streamlines and interface shapes for $Ca = 0.6$ and $\rho_d/\rho_s = 6/5$.

3.3. *Falling drops*, $0.6 \leqslant Ca \leqslant 1.0$

Streamlines for $Ca = 0.6$ are presented in figure 18. At $Re = 0$, the drop is decidedly more prolate ($\alpha = 0.92$) than in previous cases. By $Re = 4$, substantial departure from sphericity is noticeable. As Re increases, the drop deforms oblately and its wing-tip is swept back by the flow, as shown for $Re = 10$ and 18. Although the drop has deformed significantly by $Re = 18$, we do not find a disjoint recirculation zone, as seen for smaller Ca. A factor that might contribute to the absence of the disjoint recirculation zone is the inability of the drop to maintain a high frontal area, owing to low interfacial tension. We note that the maximum frontal area $A_{frontal} \approx 1.25$ (at $Re = 18$) is much lower than the maximum values (as high as 2.25) shown above for comparable degrees of deformation.

Figures 19(*a*)–19(*d*) show that C_D, α, $A_{frontal}$, and $A_{surface}$ increase or decrease monotonically with Re. In figure 19(*a*), we see that C_D decreases rapidly until $Re \approx 10$, beyond which it seems to approach a constant value of $C_D \approx 8$. Figure 19(*b*) shows α increasing, with $\mathrm{d}^2\alpha/\mathrm{d}(Re)^2 < 0$. Figure 19(*c*) shows a nearly linear increase of $A_{frontal}$ with Re. Figure 19(*d*) shows that $A_{surface}$ increases, with $\mathrm{d}^2 A_{surface}/\mathrm{d}(Re)^2 > 0$.

For $Ca = 1.0$ figure 20 shows streamlines for increasing Re. At $Re = 0$, the drop is significantly prolate ($\alpha = 0.89$) with fore–aft asymmetry. By $Re = 2.4$, we find a deformed rear-indented drop with $A_{frontal} = 0.94$. Qualitatively, the flow changes

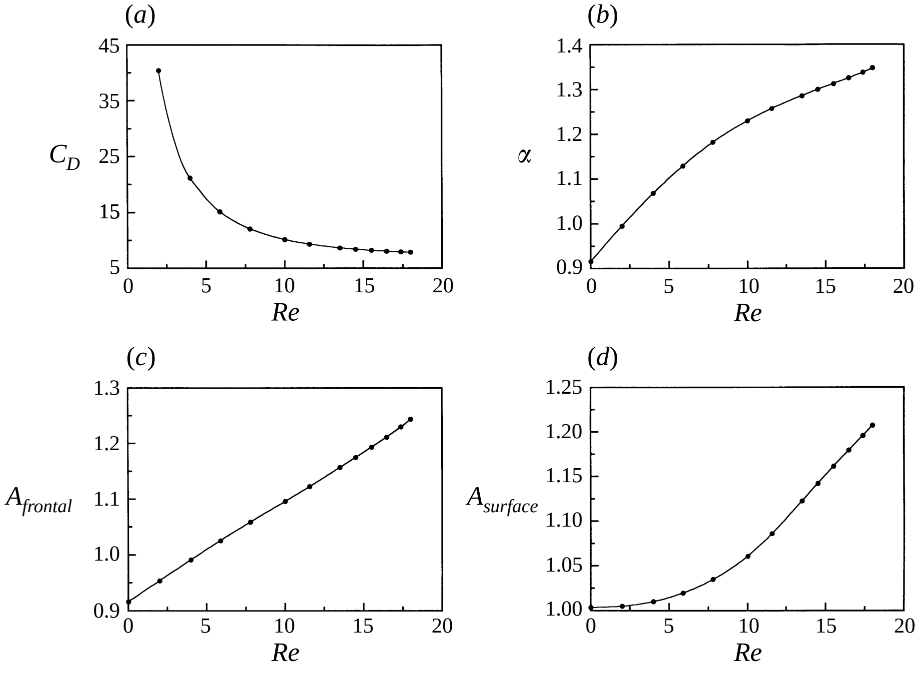

FIGURE 19. Variation of integral properties with Re for $Ca = 0.6$ and $\rho_d/\rho_s = 6/5$. (a) C_D; (b) α; (c) $A_{frontal}$; (d) $A_{surface}$.

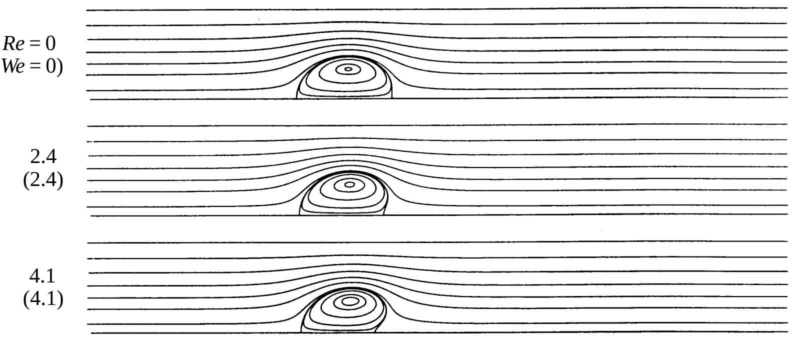

FIGURE 20. Streamlines and interface shapes for $Ca = 1.0$ and $\rho_d/\rho_s = 6/5$.

very little until at least $Re = 4.1$, barring slight variation in $A_{frontal}$, which is 0.97 at $Re = 4.1$. The integral measures for $Ca = 1.0$ are very similar to those presented for $Ca = 0.6$.

3.4. *Rising drops*

For the rising case, we consider $\mu_d/\mu_s = 1$, $R_d/R_t = 0.5$, and $\rho_d/\rho_s = 5/6$. When ρ_d/ρ_s is near unity, one expects similar results for falling or rising drops, since ρ_d/ρ_s appears only as a coefficient in the momentum equation (1*a*), and for $\rho_d/\rho_s \approx 1$ that coefficient is an $O(1)$ quantity. With these parameters, we computed flows for each Ca presented in §§3.1–3.3 and found them to be qualitatively similar, with the integral measures differing by no more than a few per cent from those shown in figures 11(*a*)–11(*d*). Here we present one such series to illustrate these similarities.

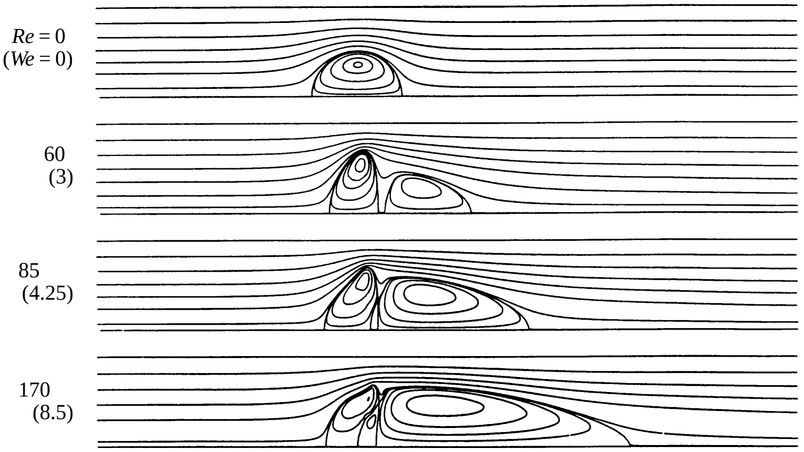

FIGURE 21. Streamlines and interface shapes for $Ca = 0.05$ and $\rho_d/\rho_s = 5/6$.

Figure 21 shows streamlines for the rising case with $Ca = 0.05$. The vertically upward drop motion is depicted as a left-to-right flow of the suspending liquid in the drop-fixed frame. At $Re = 0$, the drop is slightly prolate ($\alpha = 0.9978$). As for the falling cases, the drop deforms oblately with increasing Re. A disjoint recirculation zone appears by $Re = 60$, and the forward stagnation point of the disjoint recirculation zone crosses the drop interface by $Re = 85$. The highly deformed drop shown for $Re = 170$ is quite similar to the corresponding falling case shown for the same Re in figure 10. Finally, figure 22 shows that the finite-element mesh used to compute the flow shown for $Re = 170$ is still reasonably orthogonal. Such maintenance of approximate mesh orthogonality, and further improvement, when needed, can be achieved by 'tuning' the local values of D_ξ and D_η in (11).

4. Discussion

4.1. *Comparison to previous theoretical and experimental results*

In the limit $Re = 0$, our code allows for comparison to the approximate analytical results of Haberman & Sayre (1958) and the calculations of Coutanceau & Thizon (1981). Haberman & Sayre (1958) used a functional expansion to represent Stokes flow of an undeformed spherical drop falling in a vertical tube, retaining only the two terms satisfying boundary conditions on the undeformed interface. In our notation, their expression (the terminal velocity U was inadvertently omitted from the right-hand side of equation (74) of Haberman & Sayre (1958)) for the drag force is

$$F_{D,\,Stokes,\,sphere,\,tube} = 6\pi\mu_s R_d\, U\frac{2+3(\mu_d/\mu_s)}{3+3(\mu_d/\mu_s)}K_1, \tag{28}$$

where K_1 (whose dependence on the viscosity ratio and radius ratio is given in equation 9–29 of Clift *et al.* (1978)) is defined as $K_1 = F_{D,\,Stokes,\,sphere,\,tube}/F_{D,\,Stokes,\,sphere,\,\infty}$, where the numerator and denominator are the drag forces for creeping flow of a spherical drop in a finite tube and an unbounded domain, respectively. For $R_d/R_t = 0.5$ and equal viscosities, the analysis of Haberman & Sayre gives $K_1 = 4.0911$. In contrast, the Stokes flow calculations of Coutanceau & Thizon (1981), which provide a non-singular

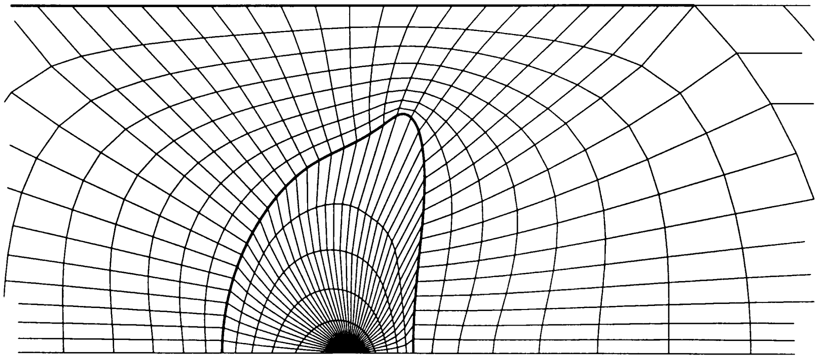

FIGURE 22. Finite-element mesh near the drop for $Ca = 0.05$, $Re = 170$ ($We = 8.5$), and $\rho_d/\rho_s = 5/6$. The interface is shown in bold.

description of the far-field flow and a more accurate representation of the near-field, give $K_1 = 4.120$. For the same parameter values, we have set $Re = 0, Ca = 0.001$ (for which little deformation occurs for $R_d/R_t = 0$ at small Re), $\rho_d/\rho_s = 6/5$, and calculated the ratio of the computed $F_D = \frac{4}{3}\pi\mu_s UR_d St$ to the Stokes drag in an unbounded domain, finding $F_D/F_{D, Stokes, sphere, \infty} = 4.1199$. (For $\rho_d/\rho_s \neq 1$, the density ratio in our calculation is of no consequence as $Re \rightarrow 0$, in which limit our governing equations, save (4), are independent of ρ_d/ρ_s; note that $\rho_d/\rho_s = 1$ is a singular case since $St = 0$.) We also repeated the computation with a coarser mesh (560 elements) and found $K_1 = 4.1199$, thus suggesting that our results are converged as the mesh is refined.

As discussed in §1, there is only very limited experimental data for falling or rising drops in tubes at Reynolds numbers in excess of unity (Strom & Kintner 1958; Harmathy 1960; Salami, Vignes & Le Goff 1965; O'Brien 1969). The only report of drop shape is that of O'Brien (1969), whose results are restricted to $R_d/R_t > 1$. We can, however, make some limited comparison to terminal velocity measurements. Salami *et al.* (1965) have reported terminal velocities for carbon tetrachloride drops of three sizes falling through water in different tubes with $R_d/R_t \simeq 0.5$. For the smallest drop (smallest Re) the measured terminal velocity, equivalent drop radius, and reported viscosities ($\mu_d/\mu_s = 0.97$) give $Re = 320$, $C_a = 0.0019$, and $C_D = 3.816$. For $\mu_d/\mu_s = 1$, $R_d/R_t = 0.5, \rho_d/\rho_s = 1.59$, and these values of Re and Ca, we compute $C_D = 0.4117$ for axisymmetric steady drop descent. We note that the experimental value is greatly in excess of both our computed C_D and the C_D for either a rigid sphere or an oblate spheroid with the same axis ratio at this Re (Clift *et al.* 1978, pp. 226–8, and references cited therein). Conversely, the measured vertical speed is much lower than that which would be predicted for steady vertical descent of a rigid sphere or an oblate spheroid having the same mass and diameter. Since C_D for a drop with a mobile interface is expected to be smaller than that of a rigid body having the same shape, we can conclude that the high C_D of Salami *et al.* does not correspond to axisymmetric steady motion of a drop whose interface is rendered immobile by contamination. Thus, the greatly reduced rate of descent would appear to be due to significant trajectory meandering, possibly involving close approaches to the tube wall. The data of Salami, *et al.* (1965) thus suggest that drop motion in their experiments was not vertical. This hypothesis is consistent with the experimental work of Magarvey & Bishop (1960, 1961*a*, *b*), whose experiments with the same dispersed and suspending liquids in this range of Re in an essentially unbounded domain revealed unsteady non-axisymmetric flow and drop trajectories exhibiting large horizontal excursions. Given the apparent unsteady and non-axisymmetric nature of the flow inferred for drops with $Re = 320$, we have made no comparison to the two larger carbon tetrachloride drops considered by Salami *et al.* (1965). Note that none of the papers cited as references for the data in figure 9.4 of Clift *et al.* (1978) discusses near-collisions with the wall, even though Reynolds numbers as high as 1000 were considered.

With respect to the availability of drop shape data, the situation without wall effects is only slightly better. With the exception of the work of Winnikow & Chao (1966) for bromobenzene drops in water (see §2.2), all data known to us were obtained for liquid pairs with large viscosity contrast, or in experiments where the liquids were insufficiently purified. Impurities lead to relatively immobile interfaces, and hence to higher values of C_D. For example, Winnikow (1965; figure 16) shows that for bromobenzene drops in water, the C_D values obtained using triply distilled water and the middle fraction of doubly distilled bromobenzene are as much as 70% less than those of earlier workers using less thoroughly purified liquids. We also note that interfacial immobility can have significant effects on drag, while altering the axis ratio only slightly. To illustrate, we consider the extensive data of Wellek *et al.* (1966), who used laboratory distilled water and singly-distilled organic liquids. These authors observed carbon tetrachloride drops of one size falling through water ($\mu_d/\mu_s = 1.047$), water drops of three sizes falling through chlorobenzene ($1.111 \leqslant \mu_d/\mu_s \leqslant 1.125$), and cyclohexane drops of six sizes rising through water ($\mu_d/\mu_s = 0.978$). From tabulations of terminal velocity, eccentricity, densities, and viscosities, we have calculated Re ($440 \leqslant Re \leqslant 821$) and Ca ($0.002 \leqslant Ca \leqslant 0.007$), and have computed α and C_D using $R_d/R_t = 0.1$ (with 727 elements). In each case, our computed axis ratio compares well to experiment, exceeding the experimental value by between 1 and 4% (mean deviation 2.3%). However, the computed drag coefficients lie 50–75% below the experimental values. For example, for 0.350 cm cyclohexane drops rising in water ($Re = 532, Ca = 0.0030$), we use the reported density and viscosity ratios and find $\alpha = 1.15$ and $C_D = 0.181$, compared to experimental values of 1.13 (tabulated) and 0.547 (computed from the terminal velocity and other tabulated data). In general, the experimental drag coefficients lie close to the 'standard drag curve' for rigid spheres (cf. Clift *et al.* 1978). Similar calculations for the cyclohexane-in-water data of Keith & Hixson (1955; $\mu_d/\mu_s = 0.98$) reveal comparable discrepancies (i.e. by a factor of three or more) between our computed drag coefficients and experimental values. These results are consistent with a less than fully mobile interface.

Thus, we see that our computations can be used to identify experimental data in which conditions deviate from steady, vertical motion of a drop with a completely mobile interface. In some cases, the results allow inferences to be drawn about the source of the discrepancy.

4.2. *Topology of the flow*

The flows described in §3 differ in several qualitative aspects from previous non-zero-Re drop computations (Dandy & Leal 1989; Haywood, Renksizbulut & Raithby 1994*a*, *b*). First, they show a considerably greater degree of drop deformation. Secondly, they clearly demonstrate that a disjoint recirculation zone of the type found by Dandy & Leal (1989) sometimes attaches to the drop as Re is increased, and that this is followed by division of the drop into two adjacent recirculating regions. Thirdly, our results show how a second (smaller) external recirculation zone can develop between the rear of the drop and the front of the (larger) primary external recirculation zone. These points are discussed below. Heat and mass transfer consequences of these features and of the non-monotonic dependence of axis ratio on Re are discussed in §4.4.

The highly oblate drops shown in § 3 include quasi-ellipsoidal as well as highly non-convex shapes. The former class has been discussed in the unbounded case by Dandy & Leal (1989). For $R_d/R_t = 0.5$, the shapes and flow fields are similar, with significant differences expected for larger values of R_d/R_t. The highly non-convex drop shapes do not have counterparts in any of the previous calculations, the only non-convex drop-shape computations known to us being those shown in figures 2 and 3 of Dandy & Leal (1989) for $Re = 2$ and 10. For $Re = 2$, $\mu_d/\mu_s = 4$, and $\rho_d/\rho_s = 0.909$, Dandy & Leal show a sequence of drop shapes at high Ca ($Ca \geqslant 2$) similar to, but less deformed than those shown in our figures 15 (for $Re = 8$ and 25) and 18 (for $Re = 4$, 10 and 18). The non-convex drops shown in figures 15 (for $Re = 25, 30, 40, 50$ and 75) and 18 (for $Re = 18$), and the increasing non-convexity as Re increases are reminiscent of water drops photographed in air by Pruppacher & Beard (1970), and are suggestive of development of 'skirted' drop shapes that give rise to unsteadiness and drop breakup (Clift *et al.* 1978).

In figures 3, 5, 7, 10 and 12 we show how a disjoint recirculation zone developes in the suspending liquid in the wake of the drop, as previously described by Dandy & Leal (1989). For $Ca = 0.2$ and $50 < Re < 150$, the length of this zone (see figure 13) exceeds that of the separated flow region in the wake of a rigid sphere (Taneda 1956). The front of the disjoint recirculation zone moves towards the rear of the drop and attaches (i.e. the recirculating fluid in the disjoint separated flow of the suspending liquid contacts the drop), as shown in figure 13. This attachment corresponds to coincidence of the forward stagnation point (z_{s1}) of the disjoint recirculation zone with the rear stagnation point of the drop. As Re increases, an internal stagnation point develops on the symmetry axis, and the streamsurface connecting that internal stagnation point to the separation circle on the interface effectively divides the drop into two adjacent recirculation zones. Two distinct recirculation zones (topologically, vortex rings in this flow) have previously been described by Pruppacher & Beard (1970) in the context of a nearly spherical water drop ($Re = 135$) suspended in a vertical wind tunnel, and computed by Rivkind & Ryskin (1976) for undeformed spherical drops. The only other observation known to us of two distinct vortex rings inside a drop is that of Wairegi (1974), who reported a very thin internal recirculation zone running from the rear stagnation point to the 'hemline' of a highly deformed skirted drop (see figure 8.5 of Clift *et al.* 1978). That the development of a disjoint recirculation zone does not depend on drop deformation is apparent from the numerical results of Rivkind & Ryskin (1976), whose calculations did not admit deformation, and those of Dandy & Leal (1989), whose figure 5 shows the presence of such a zone in the wake of a nearly spherical drop.

As discussed in § 3.2, a second recirculation zone in the suspending fluid (external to the drop), shown in figure 15 for $Ca = 0.2$, develops by closure of a streamsurface that follows the drop interface to the symmetry axis, follows the axis to the forward stagnation point of the large ('primary') disjoint recirculation zone, and then follows, radially outward and subsequently downstream, the streamsurface separating the primary external recirculation zone from the bulk of the suspending fluid. To the best of our knowledge, such a second closed recirculation zone in the suspending fluid has not been reported previously. The flow fields shown in figure 18 suggest that such a secondary external recirculation zone will also develop at higher Re for $Ca = 0.6$. The streamline plots indicate that this feature of the flow is critically dependent on deformation of the drop, unlike development of the first external recirculation zone, which is apparent in the undeformed drop calculations of Rivkind & Ryskin (1976).

Finally, we note that, as shown in §§ 3.1–3.3, the drop shape at $Re = 0$ is increasingly prolate as Ca increases from zero (at which value the drop is spherical). In light of the required sphericity of drops at $Re = 0$ in an unbounded flow, this is clearly an effect of the wall.

4.3. *Experimental implications*

Several factors will determine the experimental realizability of the results described in §3. Among these are stability, availability of liquids with the desired physical properties, and the reachability of these steady axisymmetric solutions from some set of initial conditions (i.e. injection of a drop into a liquid in a tube).

In the unbounded case, several experimental studies have shown that as Re increases, the steady axisymmetric motion of a drop becomes unstable, leading to either oscillatory non-axisymmetric behaviour or axisymmetric breakup (Grace *et al.* 1978). In the latter case, creeping flow experiments and analysis by Koh & Leal (1990) and Pozrikidis (1990) show that breakup can occur through growth of axisymmetric disturbances. In the geometry considered here, we also expect instability to occur at sufficiently high Re.

The results of Winnikow & Chao (1966) for thoroughly purified liquids show that in an unbounded domain, axisymmetric drop motion can be achieved for Re as high as 876, well beyond the values at which axisymmetric motion of nearly spherical drops with immobile interfaces (Magarvey & Bishop 1960, 1961*a*, *b*; Magarvey & MacLatchy 1965) becomes unstable. This is consistent with the absence of, in the case of highly purified liquids and a fully mobile interface, a shear-layer type instability mode localized near the equator. This instability has been discussed for rigid spheres by Kim & Durbin (1988) and Kim & Pearlstein (1990). We believe it to be the dominant instability mode observed experimentally for rigid spheres in the range $130 < Re < 290$ (Möller 1938; Taneda 1956; Roos & Willmarth 1971; Goldburg & Florsheim 1966), as well as for nearly spherical drops with presumably immobile interfaces (Magarvey & Bishop 1960, 1961*a*, *b*; Magarvey & MacLatchy 1965). For drops, suppression of an equatorial shear-layer type instability should be most pronounced in the case of 'clean' mobile interfaces, for which the shear stress is continuous across the interface. We thus hypothesize that the onset of instability observed by Winnikow & Chao (1966) for four liquid pairs in the range $686 < Re < 876$ is a wake instability (Kim & Durbin 1988). We conjecture that for homoviscous liquid pairs, for which not only the shear stress, but also the shear rate, is continuous across the interface, onset will occur at higher Re than when a viscosity mismatch obtains. Computations for a sphere fixed in a tube (Tavener 1994) and an unbounded flow (Natarajan & Acrivos 1993) show that the first instability corresponds to steady bifurcation (near $Re = 210$) to a non-axisymmetric mode localized in the wake, but the implications for the stability of a drop with a fully mobile interface rising or falling in a liquid with comparable density and viscosity are not clear. Stability of drop motions can, in principle, be studied either by an eigenvalue/eigenmode approach or by direct integration of the axisymmetric (e.g. Foote 1975; Kang & Leal 1987; Takagi, Matsumoto & Huang 1995) or non-axisymmetric (e.g. Unverdi & Tryggvason 1992; Lafaurie *et al.* 1994) dynamical equations.

It is well known that the trajectories of drops and bubbles moving under the action of gravity in an unbounded flow can deviate from the vertical (Hartunian & Sears 1957; Magarvey & Bishop 1960, 1961*a*, *b*; Satapathy & Smith 1961; Magarvey & MacLatchy 1965; Duineveld 1995). Moreover, we note that the effect of mean shear on the radial migration of drops in circular Poiseuille flow (cf. Hetsroni, Haber & Wacholder 1970; Olbricht & Kung 1992) is absent when the flow is driven by buoyancy alone. Thus, we speculate that instability will give rise to significant trajectory meandering, and that, unless $R_a/R_t \ll 1$, near-collisions with the tube wall will result at sufficiently high *Re*.

Since nearly homoviscous and nearly homopycnic immiscible liquid pairs are easily obtained (cf. Olbricht & Kung 1992), it is clear that immiscible liquid pairs with equal viscosity and different densities can also be obtained. The reduced tendency of the drop trajectory to coincide with the tube axis will require more careful injection and centring, relative to drop motion in a circular Poiseuille flow.

4.4. *Consequences for heat and mass transfer*

The flow fields shown and described in §3 have important consequences for heat and mass transfer to or from drops. These consequences are due primarily to internal circulation within the drop, effective division of the drop into two distinct adjacent vortices, development of one or two closed recirculation zones in the suspending liquid, and the increased surface area that necessarily accompanies deformation. To date, the only heat or mass transfer calculations known to us for deformable drops are the recent quasi-steady and fully transient calculations of Haywood *et al.* (1994*a*, *b*) for evaporating hydrocarbon drops in air ($\rho_a/\rho_s \gg 1$ and $\mu_a/\mu_s \gg 1$), even though several authors have commented on the importance of deformation in applications (cf. Sirignano 1983, 1993).

Internal circulation increases transport rates by virtue of increasing the drop-side transport rate over its nominal value in the absence of internal flow (Garner & Tayeban 1960*a*, *b*; Walcek & Pruppacher 1984). We note that in the homoviscous case, the primary effect of the drop interface is to establish a material interface across which (i) no motion occurs (in a frame moving with the drop), and (ii) the pressure is discontinuous. The absence of tangential surface tension variation leads to continuity of the tangential stress across the interface, and in the homoviscous case, continuity of the tangential shear. Thus, in the homoviscous case, the velocity field advecting a scalar inside and outside the drop is not only continuous across the interface, but also differentiable. Hence, as *Re* (and thus the Péclet number† $Pe = RePr$, where *Pr* is the Prandtl number) increases, we expect the temperature field to be relatively smoother across the interface than for $\mu_a/\mu_s \neq 1$. Note that a similar result will not obtain for mass transfer processes in which the partition coefficient differs from unity, in which case the concentration itself will be discontinuous across the interface.

Division of the drop volume into two distinct recirculating vortices separated by a streamsurface across which no flow occurs would seem to have the effect of reducing the efficiency of drop-side convective mixing by a degree dependent upon the internal Péclet number and the size of the second internal recirculation zone. For small *Pe* or a small second zone, one would expect relatively little effect on drop-side transfer rates, while for large *Pe* or a larger recirculation zone, significant effects may occur.

We expect that development of a large disjoint recirculation zone downstream of the drop will have important consequences in some applications. As can be inferred from the discussion of Garner & Tayeban (1960*a*, *b*) for the unbounded case, the magnitude of the effects will depend on the direction of transport (i.e. from the suspending liquid to the drop or vice versa). For example, in the mobilization of oil drops by water flooding and surfactant addition in tertiary oil recovery, one may expect that surfactant that has diffused away from the aqueous/organic interface will accumulate in the disjoint recirculation zone, where its concentration is likely to be higher than in

---

† Note that in the homoviscous case, the internal and external Reynolds numbers differ by the density ratio.)

the remainder of the aqueous phase. Similar considerations will apply to the unbounded case, in which significant accumulation of species may also occur in the disjoint recirculation zone. The capacity of external recirculation zones to accumulate species in the suspending liquid, where they are advected with the drop, depends on volume (Kalra & Uhlherr 1973). On the other hand, the rate of transfer to or from the external recirculation zones depends on area. It is also clear that one or more external recirculation zones can affect the overall rates of transport processes. One example is the concentration of trace gases and particulate in the wakes of large raindrops falling through polluted atmospheric strata. With the assumption of a spherical drop, Walcek & Pruppacher (1984) computed the overall rate of absorption of sulphur dioxide by falling water drops in air at $Re = 100$ (cf. figure 10-21 of Pruppacher & Klett 1978). It is clear from their treatment that overall transport rates (including systems with chemical reactions, such as that considered by Walcek & Pruppacher) will be significantly affected by drop deformation, by the considerably more complex internal flow that can occur when deformation is allowed, and by the presence of one or more external recirculation zones.

Finally, as discussed in the mass transfer context by Keith & Hixson (1955) and Garner & Tayeban (1960*a*), increased interfacial area resulting from drop deformation can significantly affect mass transfer. The extent to which heat or mass transfer is enhanced depends on the fractional increase in contact area, and on the nature of flow inside and outside the drop. Thus, the extent to which drop deformation is associated with interfacial area variation is an important consideration in predicting transport rates. As shown in §3, the variation of interfacial area (normalized by the area of a sphere of equal volume) is sometimes non-monotonic. Whether this can lead to non-monotonic variation of the mass transfer rate with Re is an open question.

Helpful discussions with Professors B. T. Chao, L. G. Leal, W. L. Olbricht, and C. Pozrikidis, and Drs M. J. Martinez, V. O'Brien and E. J. Stern are gratefully acknowledged. We thank W. J. Mantle for assistance in plotting and M. Schwartz for providing a copy of the paper by Kilgore. This work was supported by NASA Grant NGT-51360 and NSF Grant CTS-9422770 to the University of Illinois, and in part by the Division of Engineering and Geosciences, Office of Basic Energy Sciences, US Department of Energy, under contract DE-AC05-840R21400 with Martin Marietta Energy Systems, Inc. The authors gratefully acknowledge access to computational facilities provided by the IBM Corporation under the auspices of the Shared University Research Program.

REFERENCES

BAUMANN, N., JOSEPH, D. D., MOHR, P. & RENARDY, Y. 1992 Vortex rings of one fluid in another in free fall. *Phys. Fluids* A **4**, 567–580.

BEARD, K. V. 1976 Terminal velocity and shape of cloud and precipitation drops aloft. *J. Atmos. Sci.* **33**, 851–864.

BRENNER, H. 1971 Pressure drop due to the motion of neutrally buoyant particles in duct flows. II. Spherical droplets and bubbles. *Ind. Engng Chem. Fund.* **10**, 537–543.

BRUNSON, R. J. & WELLEK, R. M. 1970 Mass transfer within oscillating liquid droplets. *Can. J. Chem. Engng* **48**, 267–274.

BUCKMASTER, J. D. & FLAHERTY, J. E. 1973 The bursting of two-dimensional drops in slow viscous flow. *J. Fluid Mech.* **60**, 625–639.

CHEN, J., DAGAN, Z. & MALDARELLI, C. 1991 The axisymmetric thermocapillary motion of a fluid particle in a tube. *J. Fluid Mech.* **233**, 405–437.

Christodoulou, K. N. 1990 Computational physics of slide coating flow. PhD thesis, University of Minnesota.

Christodoulou, K. N. & Scriven, L. E. 1989 The fluid mechanics of slide coating. *J. Fluid Mech.* **208**, 321–354.

Christodoulou, K. N. & Scriven, L. E. 1992 Discretization of free surface flows and other moving boundary problems. *J. Comput. Phys.* **99**, 39–55.

Clift, R., Grace, J. R. & Weber, M. E. 1978 *Bubbles, Drops, and Particles.* Academic.

Coutanceau, M. & Thizon, P. 1981 Wall effect on the bubble behaviour in highly viscous liquids. *J. Fluid Mech.* **107**, 339–373.

Crabtree, J. R. & Bridgwater, J. 1969 Chain bubbling in viscous liquids. *Chem. Engng Sci.* **24**, 1755–1768.

Dandy, D. S. & Leal, L. G. 1989 Buoyancy-driven motion of a deformable drop through a quiescent liquid at intermediate Reynolds numbers. *J. Fluid Mech.* **208**, 161–192.

Duineveld, P. C. 1995 The rise velocity and shape of bubbles in pure water at high Reynolds number. *J. Fluid Mech.* **292**, 325–332.

Dukler, A. E., Fabre, J. A., McQuillen, J. B. & Vernon, R. 1988 Gas–liquid flow at microgravity conditions: flow patterns and their transitions. *Intl J. Multiphase Flow* **14**, 389–400.

Dwyer, H. A. 1989 Calculations of droplet dynamics in high temperature environments. *Prog. Energy Combust. Sci.* **15**, 131–158.

Eiseman, P. R. 1982*a* Coordinate generation with precise controls over mesh properties. *J. Comput. Phys.* **47**, 331–351.

Eiseman, P. R. 1982*b* High level continuity for coordinate generation with precise controls. *J. Comput. Phys.* **47**, 352–374.

Faeth, G. M. 1983 Evaporation and combustion of sprays. *Prog. Energy Combust. Sci.* **9**, 1–76.

Fararoui, A. & Kintner, R. C. 1961 Flow and shape of drops in non-Newtonian fluids. *Trans. Soc. Rheol.* **5**, 369–380.

Feng, J. Q. & Basaran, O. A. 1994 Shear flow over a translationally symmetric cylindrical bubble pinned on a slot in a plane wall. *J. Fluid Mech.* **275**, 351–378.

Foote, G. B. 1975 The water drop rebound problem: dynamics of collision. *J. Atmos. Sci.* **32**, 390–402.

Garner, F. H. & Tayeban, M. 1960*a* The importance of the wake in mass transfer from both continuous and dispersed phase systems. I. *Anales de la Real Sociedad Española de Física y Química* **56**(B), 479–490.

Garner, F. H. & Tayeban, M. 1960*b* The importance of the wake in mass transfer from both continuous and dispersed phase systems. II. *Anales de la Real Sociedad Española de Física y Química* **56**(B), 491–498.

Goldburg, A. & Florsheim, B. H. 1966 Transitions and Strouhal number for the incompressible wake of various bodies. *Phys. Fluids* **9**, 45–50.

Grace, J. R. 1983 Hydrodynamics of liquid drops in immiscible liquids. In *Handbook of Fluids in Motion* (ed. N. P. Cheremisinoff & R. Gupta), chap. 38. Ann Arbor Science.

Grace, J. R., Wairegi, T. & Brophy, J. 1978 Break-up of drops and bubbles in stagnant media. *Can. J. Chem. Engng* **56**, 3–8.

Haberman, W. L. & Sayre, R. M. 1958 *Motion of Rigid and Fluid Spheres in Stationary and Moving Liquids inside Cylindrical Tubes.* David Taylor Model Basin Report 1143.

Hadamard, J. S. 1911 Mouvement permanent lent d'une sphère liquide et visqueuse dans un liquide visqueux. *C. R. Acad. Sci.* **152**, 1735–1738.

Happel, J. & Brenner, H. 1965 *Low Reynolds Number Hydrodynamics.* Prentice-Hall.

Harmathy, T. Z. 1960 Velocity of large drops and bubbles in media of infinite or restricted extent. *AIChE J.* **6**, 281–288.

Hartunian, R. A. & Sears, W. R. 1957 On the instability of small gas bubbles moving uniformly in various liquids. *J. Fluid Mech.* **3**, 27–47.

Haywood, R. J., Renksizbulut, M. & Raithby, G. D. 1994*a* Transient deformation and evaporation of droplets at intermediate Reynolds numbers. *Intl J. Heat Mass Transfer* **37**, 1401–1409.

Haywood, R. J., Renksizbulut, M. & Raithby, G. D. 1994*b* Numerical solution of deforming evaporating droplets at intermediate Reynolds numbers. *Numer. Heat Transfer* A **26**, 253–272.

Hetsroni, G., Haber, S. & Wacholder, E. 1970 The flow fields in and around a droplet moving axially within a tube. *J. Fluid Mech.* **41**, 689–705.

Hewitt, G. F. & Hall-Taylor, N. S. 1970 *Annular Two-Phase Flow*. Pergamon.

Ho, B. P. & Leal, L. G. 1975 The creeping motion of liquid drops through a circular tube of comparable diameter. *J. Fluid Mech.* **71**, 361–383.

Hood, P. 1976 Frontal solution program for unsymmetric matrices. *Intl J. Num. Meth. Engng* **10**, 379–399. [See *ibid.* **11**, 1055 (1977) for corrigendum.]

Huyakorn, P. S., Taylor, C., Lee, R. L. & Gresho, P. M. 1978 A comparison of various mixed interpolation finite elements in the velocity-pressure formulation of the Navier–Stokes equations. *Comput. Fluids* **6**, 25–35.

Kalra, S. P. 1990 On the methodology for assessing steam generator tube rupture safety margins. *Nucl. Safety* **31**, 187–201.

Kalra, T. R. & Uhlherr, P. H. T. 1973 Mass transfer between the attached wake of a bluff body and the free stream. *Chem. Engng Sci.* **28**, 915–923.

Kang, I. S. & Leal, L. G. 1987 Numerical solution of axisymmetric, unsteady free-boundary problems at finite Reynolds number. I. Finite-difference scheme and its application to the deformation of a bubble in a uniaxial straining flow. *Phys. Fluids* **30**, 1929–1940.

Keith, F. W. & Hixson, A. N. 1955 Liquid–liquid extraction spray columns. *Ind. Engng Chem.* **47**, 258–267.

Keller, H. B. 1977 Numerical solution of bifurcation and nonlinear eigenvalue problems. In *Applications of Bifurcation Theory* (ed. P. Rabinowitz), pp. 359–384. Academic.

Kilgore, L. C. 1971 Bubble retention and fluid flow in MLB through-holes. *Ann. Symp. California Circuits Assn.* Los Angeles, CA, 10–11 Nov., 1971.

Kim, H. J. & Durbin, P. A. 1988 Observations of the frequencies in a sphere wake and of drag increase by acoustic excitation. *Phys. Fluids* **31**, 3260–3265.

Kim, I. & Pearlstein, A. J. 1990 Stability of the flow past a sphere. *J. Fluid Mech.* **211**, 73–93.

Kistler, S. F. & Scriven, L. E. 1983 Coating flows. In *Computational Analysis of Polymer Processing* (ed. J. R. A. Pearson and S. M. Richardson), pp. 243–299. Applied Science.

Koh, C. J. & Leal, L. G. 1990 An experimental investigation on the stability of viscous drops translating through a quiescent fluid. *Phys. Fluids* A **2**, 2103–2109.

Krabach, M. H., Donnelly, R. G., Reber, S. A. & Davis, G. J. 1977 The kinetics of deaeration of seawater by gas sparging in a cross-flow flume. *Ind. Engng Chem. Fund.* **16**, 430–439.

Lafaurie, B., Nardone, C., Scardovelli, R., Zaleski, S. & Zanetti, G. 1994 Modelling merging and fragmentation in multiphase flows with SURFER. *J. Comput. Phys.* **113**, 134–147.

Law, C. K. 1982 Recent advances in droplet vaporization and combustion. *Prog. Energy Combust. Sci.* **8**, 171–201.

Le Clair, B. P. 1970 Viscous flow in multiparticle systems at intermediate Reynolds numbers. PhD dissertation, McMaster University, Hamilton, Ontario.

Maeda, N. 1975 Behavior of a single bubble in quiescent and flowing liquid inside a cylindrical tube. *J. Nucl. Sci. Tech.* **12**, 606–617.

Magarvey, R. H. & Bishop, R. L. 1960 The wake of a moving drop. *Nature* **188**, 735–736.

Magarvey, R. H. & Bishop, R. L. 1961*a* Transition ranges for three-dimensional wakes. *Can. J. Phys.* **39**, 1418–1422.

Magarvey, R. H. & Bishop, R. L. 1961 *b* Wakes in liquid–liquid systems. *Phys. Fluids* **4**, 800–805.

Magarvey, R. H. & MacLatchy, C. S. 1965 Vortices in sphere wakes. *Can. J. Phys.* **43**, 1649–1656.

Martinez, M. J. & Udell, K. S. 1990 Axisymmetric creeping motion of drops through circular tubes. *J. Fluid Mech.* **210**, 565–591.

Möller, W. 1938 Experimentelle Untersuchungen zur Hydrodynamik der Kugel. *Phys. Z.* **39**, 57–80.

Mudawar, I. & Deiters, T. A. 1994 A universal approach to predicting temperature response of metallic parts to spray quenching. *Intl J. Heat Mass Transfer* **37**, 347–362.

NATARAJAN, R. & ACRIVOS, A. 1993 The instability of the steady flow past spheres and disks. *J. Fluid Mech.* **254**, 323–344.

NIENOW, A. W. 1990 Gas dispersion performance in fermenter operation. *Chem. Engng Prog.* **86** (2), 61–71.

O'BRIEN, V. 1969 *Large Circulating Drops in Vertical Tubes*. Johns Hopkins University Applied Physics Laboratory Technical Memorandum TG-1084; available from National Technical Information Service as AD-697907.

OLBRICHT, W. L. & KUNG, D. M. 1992 The deformation and breakup of liquid drops in low Reynolds number flow through a capillary. *Phys. Fluids* A **4**, 1347–1354.

OLBRICHT, W. L. & LEAL, L. G. 1982 The creeping motion of liquid drops through a circular tube of comparable diameter: the effect of density differences between the fluids. *J. Fluid Mech.* **115**, 187–216.

PAYATAKES, A. C. 1982 Dynamics of oil ganglia during immiscible displacement in water-wet porous media. *Ann. Rev. Fluid Mech.* **14**, 365–393.

POZRIKIDIS, C. 1990 The instability of a moving viscous drop. *J. Fluid Mech.* **210**, 1–21.

POZRIKIDIS, C. 1992 The buoyancy-driven motion of a train of viscous drops within a circular tube. *J. Fluid Mech.* **237**, 627–648.

PRUPPACHER, H. R. & BEARD, K. V. 1970 A wind tunnel investigation of the internal circulation and shape of water drops falling at terminal velocity in air. *Q. J. R. Met. Soc.* **96**, 247–256.

PRUPPACHER, H. R. & KLETT, J. D. 1978 *Microphysics of Clouds and Precipitation*. D. Reidel, Dordrecht.

RAINA, G. K. & GROVER, P. D. 1982 Direct contact heat transfer with change of phase: theoretical model. *AIChE J.* **28**, 515–517.

RIKS, E. 1972 The application of Newton's method to the problem of elastic stability. *J. Appl. Mech.* **39**, 1060–1065.

RIVKIND, V. Y. & RYSKIN, G. M. 1976 Flow structure in motion of a spherical drop in a fluid medium at intermediate Reynolds numbers. *Fluid Dyn.* **11** (3), 5–12.

ROOS, F. W. & WILLMARTH, W. W. 1971 Some experimental results on sphere and disk drag. *AIAA J.* **9**, 285–291.

RYBCZYNSKI, W. 1911 Über die fortschreitende Bewegung einer flüssigen Kugel in einem zähen Medium. *Bull. Intl Acad. Sci. Cracovie*, *Classe des Sciences Mathematiques et Naturelles*. A *Sciences Mathematiques*, pp. 40–46.

SAITO, S. 1913 On the shape of the nearly spherical drop which falls through viscous fluid. *Sci. Rep. Tohuku Imp. Univ.*, *First Series*, **2**, 179–201.

SALAMI, E., VIGNES, A. & LE GOFF, P. 1965 Hydrodynamique des dispersions. II. Effet de paroi. Mouvement d'une goutte ou d'une bulle dans un fluide immobile contenu dans un tube vertical de petit diamètre. *Genie Chim.* **94**, 67–77.

DE SANTOS, J. M. 1991 Two-phase cocurrent downflow through constricted passages. PhD thesis, University of Minnesota.

SATAPATHY, R. & SMITH, W. 1961 The motion of single immiscible drops through a liquid. *J. Fluid Mech.* **10**, 561–570.

SCHÜGERL, K., BLASCHKE, H. G., BRUNKE, U. & STREICHER, R. 1977 Interaction of fluid dynamics, interfacial phenomena, and mass transfer in extraction processes. *Recent Developments in Separation Science* (ed. N. N. Li), 3A, pp. 71–128. CRC Press, Cleveland.

SHETH, K. S. & POZRIKIDIS, C. 1995 Effects of inertia on the deformation of liquid drops in simple shear flow. *Comput. Fluids* **24**, 101–119.

SHOPOV, P. J. & MINEV, P. D. 1992 The unsteady motion of a bubble or drop towards a liquid–liquid interface. *J. Fluid Mech.* **235**, 123–141.

SHYEH-YUNG, J. J. & STADLER, M. P. 1995 Effect of injectant composition and pressure on displacement of oil by enriched hydrocarbon gases. *SPE Reservoir Engng* **10**, 109–115.

SIRIGNANO, W. A. 1983 Fuel droplet vaporization and spray combustion theory. *Prog. Energy Combust. Sci.* **9**, 291–322.

SIRIGNANO, W. A. 1993 Fluid dynamics of sprays – 1992 Freeman Scholar Lecture. *Trans ASME* I: *J. Fluids Engng* **115**, 345–378.

STRANG, G. & FIX, G. J. 1973 *An Analysis of the Finite Element Method*. Prentice-Hall.

Strom, J. R. & Kintner, R. C. 1958 Wall effect for the fall of single drops. *AIChE J.* **4**, 153–156.

Takagi, S., Matsumoto, Y. & Huang, H. 1995 Numerical analysis of a single rising bubble using boundary-fitted coordinate system. *Trans. Japan Soc. Mech. Engrs* B **61**, 1976–1983.

Taneda, S. 1956 Experimental investigation of the wake behind a sphere at low Reynolds numbers. *J. Phys. Soc. Japan* **11**, 1104–1108.

Tavener, S. 1994 Stability of the O(2)-symmetric flow past a sphere in a pipe. *Phys. Fluids* **6**, 3884–3892.

Taylor, T. D. & Acrivos, A. 1964 On the deformation and drag of a falling viscous drop at low Reynolds number. *J. Fluid Mech.* **18**, 466–476.

Thompson, J. F., Warsi, Z. U. A. & Mastin, C. W. 1982 Boundary-fitted coordinate systems for numerical solution of partial differential equations – a review. *J. Comput. Phys.* **47**, 1–108.

Thompson, J. F., Warsi, Z. U. A. & Mastin, C. W. 1985 *Numerical Grid Generation*. Elsevier.

Tsukada, T., Hozawa, M., Imaishi, N. & Fujinawa, K. 1984 Computer simulations of deformation of moving drops and bubbles by use of the finite element method. *J. Chem. Engng Japan* **17**, 246–251.

Unverdi, S. O. & Tryggvason, G. 1992 A front-tracking method for viscous, incompressible, multi-fluid flows. *J. Comput. Phys.* **100**, 25–37.

Wairegi, T. 1974 The mechanics of large drops and bubbles moving through extended liquid media. PhD thesis, McGill University, Montreal.

Walcek, C. J. & Pruppacher, H. R. 1984 On the scavenging of SO_2 by cloud and raindrops: I. A theoretical study of SO_2 absorption and desorption for water drops in air. *J. Atmos. Chem.* **1**, 269–289.

Walters, R. A. 1980 The frontal method in hydrodynamics simulations. *Comput. Fluids* **8**, 265–272.

Weaver, R. E. C., Lapidus, L. & Elgin, J. C. 1959 The mechanics of vertical moving liquid–liquid fluidized systems: I. Interphase contacting of droplets passing through a second quiescent fluid. *AIChE J.* **5**, 533–539.

Wellek, R. M., Agrawal, A. K. & Skelland, A. H. P. 1966 Shape of liquid drops moving in liquid media. *AIChE J.* **12**, 854–862. (Supplementary tabular material available as ADI document 8768 from the Photoduplication Service, Library of Congress, Washington, DC 20540.)

Winnikow, S. R.-R. 1965 Motion and heat transfer of droplets at large Reynolds and Péclet number. PhD thesis, University of Illinois at Urbana-Champaign.

Winnikow, S. & Chao, B. T. 1966 Droplet motion in purified systems. *Phys. Fluids* **9**, 50–61.